Cerebral Cortex, November 2016;26: 4265–4281

doi: 10.1093/cercor/bhw274
Advance Access Publication Date: 9 September 2016
Original Article

ORIGINAL ARTICLE

From Shortage to Surge: A Developmental Switch in Hippocampal–Prefrontal Coupling in a Gene–Environment Model of Neuropsychiatric Disorders

Henrike Hartung[1,2], Nicole Cichon[1], Vito De Feo[1,3], Stephanie Riemann[1,7], Sandra Schildt[1], Christoph Lindemann[1], Christoph Mulert[4], Joseph A. Gogos[5,6], and Ileana L. Hanganu-Opatz[1]

[1]Developmental Neurophysiology, Institute of Neuroanatomy, University Medical Center Hamburg-Eppendorf, 20251 Hamburg, Germany, [2]Laboratory of Neurobiology, Department of Biosciences, University of Helsinki, 00014 Helsinki, Finland, [3]Laboratory of Neural Computation, Center for Neuroscience and Cognitive Systems, Istituto Italiano di Tecnologia, 38068 Rovereto, Italy, [4]Department of Psychiatry and Psychotherapy, University Medical Center Hamburg-Eppendorf, 20246 Hamburg, Germany, [5]Department of Neuroscience, Columbia University, New York, NY 10032, USA, [6]Department of Physiology, Columbia University, New York, NY 10032, USA, and [7]Current address: German Center for Neurodegenerative Diseases (DZNE), 39120 Magdeburg, Germany

Address correspondence to Ileana L. Hanganu-Opatz, Developmental Neurophysiology, Institute of Neuroanatomy, University Medical Center Hamburg-Eppendorf, Falkrenried 94, 20251 Hamburg, Germany. Email: hangop@zmnh.uni-hamburg.de

Abstract

Cognitive deficits represent a major burden of neuropsychiatric disorders and result in part from abnormal communication within hippocampal–prefrontal circuits. While it has been hypothesized that this network dysfunction arises during development, long before the first clinical symptoms, experimental evidence is still missing. Here, we show that pre-juvenile mice mimicking genetic and environmental risk factors of disease (dual-hit GE mice) have poorer recognition memory that correlates with augmented coupling by synchrony and stronger directed interactions between prefrontal cortex and hippocampus. The network dysfunction emerges already during neonatal development, yet it initially consists in a diminished hippocampal theta drive and consequently, a weaker and disorganized entrainment of local prefrontal circuits in discontinuous oscillatory activity in dual-hit GE mice when compared with controls. Thus, impaired maturation of functional communication within hippocampal–prefrontal networks switching from hypo- to hyper-coupling may represent a mechanism underlying the pathophysiology of cognitive deficits in neuropsychiatric disorders.

Key words: development, network oscillations, prefrontal cortex, schizophrenia, synchrony

Introduction

Disruption of cognitive performance in daily life represents the long-lasting burden of major neuropsychiatric disorders, such as schizophrenia (Insel 2010). Any attempt of improving the disease's outcome primarily requires the understanding of abnormalities within neuronal circuits that underlie mnemonic and

executive processing. The initially hypothesized impairment of long-range connectivity between brain areas (Wernicke 1906) has been confirmed only recently by neuroimaging and electroencephalographic studies. They identified the abnormal functional communication between the prefrontal cortex (PFC) and hippocampus (HP) as a core deficit of the disease (Meyer-Lindenberg et al. 2005; Genzel et al. 2015). The corresponding changes in neural synchronization within and between brain areas (Sigurdsson et al. 2010; Uhlhaas and Singer 2010) reflect major synaptic and cellular deficits. On the one hand, profound GABAergic dysfunction, especially in the PFC, has been related to schizophrenia (Taylor and Tso 2014; Sauer et al. 2015; Schmidt and Mirnics 2015). On the other hand, impairment of glutamate signaling (Hu et al. 2014) may equally perturb the long-range communication within hippocampal–prefrontal networks.

Recent clinical observations in prodromal cohorts led to the hypothesis that these neural circuit disturbances emerge early in life, long before the clinical manifestation of psychotic symptoms that typically occur in late adolescence and early adulthood (Cannon et al. 2003; White et al. 2006; Woodberry et al. 2008; Reichenberg et al. 2010; Uhlhaas and Singer 2011). However, the onset and developmental mechanisms of perturbation are still largely unknown. This knowledge gap is mainly due to the technical limitations of non-invasive macroscopic measurements of brain activity applicable to human infants. Animal models of neuropsychiatric disorders may represent helpful investigative tools (Nestler and Hyman 2010; Wong and Josselyn 2015), because they enable pinpointing the neuronal interactions at fine scale even at very early stages of development, which are not accessible in humans. Moreover, animal models reliably mimic the combined gene–environment etiology of the disorder and their neurobehavioral phenotypes at adulthood resemble aspects of mental illness.

Among the numerous genetic variants conferring only marginally increased risk for disease, Disrupted-in–Schizophrenia-1 (*DISC1*) represents one of the very few examples of ultra-rare mutations that have been strongly linked to neuropsychiatric disorders (Song et al. 2008, 2010; Brandon and Sawa 2011). Alone or in combination with immune challenge as environmental stressor during pregnancy, which is mimicked in mice by treatment with the viral mimetic polyriboinosinic-polyribocytidilic acid (poly I:C) (van Os et al. 2010; Meyer and Feldon 2012), *Disc1* mutations cause network dysfunction and cognitive deficits at adulthood (Kvajo et al. 2008; Abazyan et al. 2010; Kvajo et al. 2011; Cash-Padgett and Jaaro-Peled 2013; Lipina et al. 2013; Sauer et al. 2015).

Here, we aim at elucidating the developmental profile of network dysfunction and cognitive impairment in mice that recapitulate the disease-related genetic background (*Disc1* mutation), intrauterine environmental insults (poly I:C) or the combined action of both factors. To this end, we combine in vivo electrophysiology with behavioral assessment to resolve the functional communication within hippocampal–prefrontal circuits at neonatal and pre-juvenile developmental stages—the main epochs of increased circuit plasticity that have been hypothesized to be particularly prone to impairment in mental illness. We demonstrate that the patterns of neuronal activity, long-range synchrony and directed interactions within hippocampal–prefrontal networks are impaired at both developmental stages. The decreased coupling of the two areas at neonatal age switches to hyper-communication in pre-juvenile animals.

Materials and Methods

Animal Models

All experiments were performed in compliance with the German laws and the guidelines of the European Community for the use of animals in research and were approved by the local ethical committee (111/12, 132/12). Heterozygous genetically engineered mutant DISC1 mice carrying a *Disc1* allele (*Disc1*^{Tm1Kara}) on a C57Bl6/J background were used as one-hit genetic model (one-hit G). Due to two termination codons and a premature polyadenylation site, the allele produces a truncated transcript (Kvajo et al. 2008). Genotypes were determined using genomic DNA and following primer sequences: forward primer 5′-TAGCCACTCTCATTGTCAGC-3′ and reverse primer 5′-CCTCATCCCTTCCACTCAGC-3′. The offspring of pregnant dams injected i.v. at gestational day (G) 9 with the viral mimetic poly I:C (5 mg/kg) were used as one-hit environmental model (one-hit E), since they showed at adulthood deficits highly reminiscent of schizophrenia (Meyer et al. 2005; Meyer and Feldon 2012). The heterozygous offspring of DISC1 dams injected at G9 with poly I:C were used as dual-hit genetic-environmental model (dual-hit GE). Non-treated wild-type mice and the offspring of dams injected at G9 with saline (0.9 %) were used as controls. Pups were investigated during neonatal development at P8–10, the time period of maximal unidirectional hippocampal–prelimbic interactions (Brockmann et al. 2011) as well as during pre-juvenile development (P16–24). During neonatal development, the weight of pups was similar for all four groups (control: 4.9 ± 0.1 g, $n = 15$; one-hit G: 5.2 ± 0.3 g, $n = 11$; one-hit E: 4.9 ± 0.2 g, $n = 21$; dual-hit GE: 4.6 ± 0.1 g, $n = 12$, $P = 0.29$, one-way ANOVA). However, during pre-juvenile development, the body weight of dual-hit GE mice was significantly lower than that of control mice (control 10.15 ± 0.31 g; dual-hit GE 9.04 ± 0.31 g, $P = 0.02$).

Surgery

Mouse pups were initially anesthetized with isoflurane (induction 5% in O_2) followed by i.p. administration of urethane (1 g/kg body weight). The head of the pup was fixed into the stereotaxic apparatus using two small metal bars fixed with dental cement on the nasal and occipital bones, respectively. The bone over the regions of interest (prelimbic subdivision (PL) of the PFC, intermediate HP) was carefully removed by drilling holes of <0.5 mm in diameter. Removal of the dura mater by drilling was avoided, since leakage of cerebrospinal fluid or blood damps the cortical activity and neuronal firing. The body of the animal was surrounded by cotton and kept at a constant temperature of 37 °C by placing it on a heating blanket. A local anesthetic (0.25% bupivacaine/1% lidocaine) was administrated. After 20–30 min recovery period, multi-site electrodes (Neuronexus) were inserted perpendicularly to the skull surface into PL until a depth of 1.7–2.5 mm and at 20° from the vertical plane into HP at a depth of 1.2–1.7 mm. In each experiment, the electrodes were labeled with DiI (1,1′-dioctadecyl-3,3,3′,3′-tetramethyl indocarbocyanine, Invitrogen) to enable post-mortem in histological sections the reconstruction of electrode tracks in PFC and HP (Figs 2Ai,Bi and 4A,D). Two silver wires were inserted into cerebellum and served as ground and reference electrodes.

Recording Protocols

Simultaneous recordings of local field potential (LFP) and multi-unit activity (MUA) were performed from the prefrontal

subdivision PL (0.5–0.7 mm anterior to bregma and 0.3–0.5 mm from the midline) and the CA1 area of the intermediate HP (3.5–3.7 mm posterior to bregma, 3.5–3.8 from the midline) using similar protocols as described previously (Brockmann et al. 2011). One-shank Michigan electrodes with 16 recording sites (0.5–3 MΩ) that were separated by 50 µm (for HP) or 100 µm (for PL) were used. The position of recording sites over the PL and CA1 area was confirmed by post-mortem histological evaluation. Both LFP and MUA were recorded for at least 60 min at a sampling rate of 32 kHz using a multi-channel extracellular amplifier (Digital Lynx 4 S with no gain, Neuralynx) and the Cheetah acquisition software. During recording, the signal was band-pass filtered between 0.1 Hz and 5 kHz.

Data Analysis

Channels for analysis were selected on the basis of post-mortem histological investigation, that is, which recording sites of fluorescently-marked electrodes were confined to PL and hippocampal CA1, and the presence of specific patterns of activity. In the PL, these patterns were nested gamma spindle bursts (NGs) and previously characterized high-frequency oscillations (HFOs) (Brockmann et al. 2011), whereas in the HP the LFP reversal over Str. pyramidale was used for the selection of the channel with sharp waves of minimum amplitude and consequently, lowest contribution to the spectral content of the signal. Data were imported and analyzed offline using custom-written tools in Matlab software version 7.7 (Mathworks). For LFP analysis, the signals were low-pass filtered (<1500 Hz) using a third-order Butterworth filter before reducing the sampling rate to 3200 Hz. For each pup, data analysis was performed blind, that is, without knowledge of the group belonging of the pup.

The continuous pre-juvenile activity was analyzed in its amplitude, power, and spectral distribution for the entire recording. Visual inspection of spectrograms (window 10 s, overlap 80%) revealed the dominant frequency bands. Power spectral density estimates were calculated using the MATLAB function "pwelch", with a 5-s window and 50% overlap. Amplitudes of the signal filtered in different frequency bands according to the distribution in the power spectra were calculated by the root-mean-square of the filtered signal minus the mean of the filtered signal.

The detection and classification of discontinuous patterns of activity in the neonatal PL and hippocampal CA1 area were performed using a modified version of the previously-developed algorithm for unsupervised analysis of neonatal oscillations (Cichon et al. 2014) and confirmed by visual inspection. Fragmented detection of oscillations was avoided by considering events with inter-event intervals <100 ms for PL and <300 ms for HP as single events. Only oscillations lasting >1 s in PL and >1.5 s in HP and containing at least three cycles were considered for further analysis. Spindle bursts (SBs) and NGs as well as theta bursts in HP were analyzed in their occurrence (defined as the number of bursts per min), duration, maximum amplitude (defined as the voltage difference between zero and the maximal positive peak), and power distribution. The normalized power spectra were computed by dividing the total power $P(f)$ of the signal, which was band-pass filtered on frequencies f centered from 1 to 50 Hz and averaged across events of the same type, by the average baseline power spectrum $P_0(f)$ for all epochs without oscillatory activity. Peak maxima of the resulting normalized average spectra were quantified.

Time-frequency plots were calculated by transforming the LFP events using Morlet continuous wavelet. Minimal and maximal intensities in power were normalized to values between zero and one and displayed in dark blue and red, respectively.

As spectral measure of correlation between two signals coherence was calculated from the cross-spectral density and normalized by the individual power spectral density of each. The computation was performed using the magnitude-squared coherence function "mscohere" (MATLAB) based on Welch's averaged modified periodogram method (with zero overlap and 2 s time window) on 1–100 Hz filtered data according to the formula

$$C(f) = \frac{\sum_{i=1}^{N} X_i(f) Y_i^*(f)}{\sqrt{\sum_{i=1}^{N} |X_i(f)|^2 \sum_{i=1}^{N} |Y_i(f)|^2}}$$

where $X_i(f)$ and $Y_i(f)$ are the Fourier transforms of the signals x and y for the i data segment at frequency f, and * indicates the complex conjugate. The coherence coefficient is given as the modulus of the complex-valued coherence $C(f)$. For the calculation of coherence spectra from neonatal data, a continuous signal for either PL or HP was generated by concatenating multiples 2s-long segments of all co-occurring oscillatory bursts in PL and HP into single vectors. Frequency domains with significant coherence were determined by Monte Carlo simulation. For this, LFP segments of 2 s from one region were shuffled and the coherence was calculated between the shuffled LFP from one region and the original LFP from the other region. After 100 iterations, the 95th percentile of the resulting distribution was used as a significance threshold. For neonatal data, the mean coherence was calculated for all frequency components (3–8 Hz, 8–14 Hz, and 14–30 Hz) of oscillatory events that were detected as peaks in the power spectra. For pre-juvenile data, the mean coherence coefficients in the theta frequency range (4–12 Hz) were quantified.

Theta–gamma cross-frequency coupling (CFC) between LFP in PL and HP of pre-juvenile mice was calculated as previously described (Tort et al. 2010), comparing the means of modulation indices (MIs). Briefly, the signals from PL and HP were filtered in both frequency bands followed by computation of Hilbert transform to obtain the corresponding signal amplitude and phase. Subsequently, the amplitude of the theta- or gamma-filtered signal in one region was determined at each phase of filtered signal from the other region. The phase was divided into 30 bins and the mean amplitude for each bin was calculated and normalized to the total number of bins. The normalized MI was calculated as the deviation between an empirical and a uniform amplitude distribution. MI > 0 corresponds to stronger modulation, whereas MI = 0 indicates a uniform distribution of phase-amplitude values, that is, no phase-amplitude coupling. To determine whether MIs were above chance, surrogate data were generated by shifting the amplitude signal in 30 s intervals and calculating the MIs for all frequency bands. To set the MI threshold above chance level, the procedure was repeated for 100 iterations and the 95th percentile of the resulting distribution was considered as threshold.

To assess the causal interactions between PL and HP, the cross-correlation of instantaneous amplitudes of network oscillations was calculated using a modified version of a model- and spike-independent method (Adhikari et al. 2010). For this, the LFP in both regions was band-pass filtered according to the frequency band of detected coherence between PL and HP (neonatal: 3–30 Hz, pre-juvenile: 4–12 Hz). The instantaneous amplitudes of the filtered signal were calculated for time windows of co-occurring oscillations in the PL and HP. To determine the lag at which the cross-correlation peaks as well as the

magnitude of this peak, the cross-correlation between these amplitudes was calculated using a sliding-window approach (window size 4 s, step size 0.1 s). The auto-correlation (including volume conduction effects) corresponding to zero lag peak was removed by applying a pre-whitening filter. Only time windows of signal stationarity, which were above the correlation significance threshold set as

$$r_{crit} = \frac{t_{crit}}{\sqrt{(n-2)\left(1+\frac{t_{crit}^2}{n-2}\right)}} \text{ with } t_{crit} = t_{student}(n, a),\ \alpha = 0.01,$$

were considered for analysis. Only positive values were illustrated in the graphs.

To characterize the causal interactions between spike trains in neonatal PL and HP, MUA was first processed as previously described (Brockmann et al. 2011). Briefly, the raw signal was high-pass filtered (>400 Hz) and the threshold for detection of MUA was individually set depending on the geometry of the recording site. For analysis of individual spikes, the stored signals were sorted into similar waveform shapes using the Offline Sorter software (Plexon). For depicting the valid waveforms in 2D/3D space, a combination of features (including the first three principal components and peak-to-peak voltage amplitude) was chosen. Shapes of detected waveforms were visually inspected to exclude background noise. A group of similar waveforms was considered as being generated from a single neuron if it defined a discrete cluster in a 2D/3D space and exhibited a refractory period (>1 ms) in the interspike interval histograms. In a second step, the cross-correlation of spike trains from PL and HP (Brillinger 1976; Halliday and Rosenberg 1999; Siapas et al. 2005) was calculated using an algorithm modified for low firing rates and non-stationary point processes. The spiking times of individual neurons were rendered into spike train point processes of 1 ms counting interval. Due to selective occurrence of spike discharge during intermittent oscillatory activity, spike trains were non-stationary. Therefore, a sliding-window approach (window size 1 s, step size 0.1 s) was applied to all cell pairs to ensure local stationarity. For each time window, $\lambda = bTf_{Ri}f_{Rj}$ was calculated, where $f_{Ri}f_{Rj}$ is the product of the firing rates of the two spikes trains, T is the period of observation and b is the bin size. For all time windows with $\lambda > 0.1$, the cross-correlation histograms $J_{ij}^{T,b}(u)$ were computed with a bin size of 10 ms. For this, the number of spike pairs occurring at times (τ_{im}, τ_{jn}) was counted to ensure that $|\tau_{im} - \tau_{jn} - u| < b/2$ where u is the time lag. All significant bins of the histograms were averaged and smoothed by a 40-ms moving window span.

Behavioral Experiments

Testing of Exploratory Behavior and Recognition Memory

The exploratory behavior and recognition memory of control, one-hit E, one-hit G, and dual-hit GE mice were tested at pre-juvenile age using previously established experimental protocols (Kruger et al. 2012). Briefly, all behavioral tests were conducted in a circular white arena, the size of which (*D*: 34 cm, *H*: 30 cm) maximized exploratory behavior, while minimizing incidental contact with testing objects (Heyser and Ferris 2013). The objects used for testing of novelty recognition were six differently shaped, textured and colored, easy to clean items that were provided with magnets to fix them to the bottom of the arena. Object sizes (*H*: 3 cm, diameter: 1.5–3 cm) were smaller than twice the size of the mouse and did not resemble living stimuli (no eye spots, predator shape). The objects were positioned at 10 cm from the borders and 8 cm from the center of the arena. After every trial, the objects and arena were cleaned with 0.1% acetic acid to remove all odors. A black and white CCD camera (VIDEOR TECHNICAL E. Hartig GmbH) was mounted 100 cm above the arena and connected to a PC via PCI interface serving as frame grabber for video tracking software (Video Mot2 software, TSE Systems GmbH).

Exploratory Behavior in the Open Field

Pre-juvenile mice (P16) were allowed to freely explore the testing arena for 10 min. During this time grooming, rearing, wall rearing, and defecation/urination were quantified in their occurrence and duration. Additionally, the floor area of the arena was digitally subdivided in 8 zones (4 center zones and 4 border zones) using the zone monitor mode of the VideoMot 2 analysis software (VideoMot 2, TSE Systems GmbH). The time spent by pups in center and border zones as well as the running distance and velocity were quantified.

Novelty Recognition Paradigms

All protocols for assessing item recognition memory in P17–18 mice consisted of familiarization and testing trials (Ennaceur and Delacour 1988). During the familiarization trial, each mouse was placed into the arena containing two identical objects and released against the center of the opposite wall with the back to the objects. After 10 min of free exploration of objects, the mouse was returned to a temporary holding cage. In the novel object recognition (NOR) task tested in P17 mice, the first familiarization trial was followed 5 min later by a second one with identical pairs of objects. Subsequently, the test trial was performed after a delay of 5 min post-familiarization. The mice were allowed to investigate one familiar and one novel object with a different shape and texture for 5 min. Object interaction during the first minute was analyzed and compared between the groups. In the object location recognition (OLR) task, tested at P18, mice only experienced one 10 min familiarization trial with two identical objects followed after a delay of 5 min by a test trial. In the test trial, the position of one of the objects was altered. Object interaction during the first minute was analyzed and compared between the groups. In the recency recognition (RR) task, tested at P21–23, mice experienced two 10 min familiarization trials with two different sets of identical objects that were separated by a delay of 30 min. The second familiarization trial was followed after 5 min by a test trial in which one object used in the first and one object used in the second more recent familiarization trial were placed in the arena at the same positions as during the familiarization trials. Object interaction during the first minute was analyzed and compared between the groups. All trials were video-tracked and the analysis was performed using the Video Mot2 analysis software. The object recognition module of the software was used and a 3-point tracking method identified the head, the rear end and the center of gravity of the mouse. Digitally, a circular zone of 1.5 cm was created around each object and every entry of the head point into this area was considered as object interaction. Climbing or sitting on the object, mirrored by the presence of both head and center of gravity points within the circular zone, was not counted as interactions.

Statistics

Data in the text are presented as mean ± s.e.m. To facilitate the comparison between different groups and conditions, the

relative changes were calculated according to the formula for mean and variance of a ratio

$$\mathrm{Mean}\left(\frac{a}{b}\right) = \frac{\bar{a}}{\bar{b}} - \frac{\mathrm{Cov}(a,b)}{(\bar{b})^2} + \frac{\mathrm{Var}(b)\bar{a}}{(\bar{b})^3}$$

$$\mathrm{SE}\left(\frac{a}{b}\right) = \sqrt{\frac{\left(\frac{\bar{a}}{\bar{b}}\right)^2\left[\frac{\mathrm{Var}(a)}{\bar{a}^2} - 2\frac{\mathrm{Cov}(a,b)}{\bar{a}\bar{b}} + \frac{\mathrm{Var}(b)}{\bar{b}^2}\right]}{n}}$$

and displayed as bar diagrams.

Statistical analyses were performed with IBM SPSS Statistics version 21 (SPSS GmbH). Generally, all values were tested for normal distribution by the Kolmogorov–Smirnov test, except their low number ($n < 10$) precluded reliable testing. For normally distributed values, paired or unpaired *t*-test was used. For low number of values or not normally distributed values, the Shapiro–Wilk test was used. For statistics concerning the phase-locking, the CircStat Toolbox was used. Significance levels of $P < 0.05$ (*), $P < 0.01$ (**) or $P < 0.001$ (***) were detected.

Results

To mimic the disease-related genetic background, mice carrying a human-like truncating lesion in the endogenous murine *Disc1* ortholog (Kvajo et al. 2008) (DISC1 mice) were investigated as one-hit genetic model (one-hit G). DISC1 has been identified through a balanced chromosomal translocation (1;11) (q42.1; q14.3) leading to a truncation of the DISC1 gene, and segregating with schizophrenia, bipolar disorder and major depression in a large Scottish pedigree (Millar et al. 2000; Blackwood et al. 2001). Extensive characterization of adult phenotype of DISC1 mice identified the disease-related structural, functional, and cognitive deficits (Koike et al. 2006; Kvajo et al. 2008, 2011; Pletnikov et al. 2008; Brandon and Sawa 2011; Lee et al. 2013). To mimic the immune challenge during pregnancy, mice with prenatal immune activation by the viral mimetic poly I:C (Shi et al. 2003) were investigated as one-hit environmental model (one-hit E). DISC1 mice prenatally treated with poly I:C recapitulated the impact of both genetic and environmental risk factors and were considered as dual-hit gene–environment models (dual-hit GE). All investigated groups of mice (non-manipulated controls, one-hit G, one-hit E, and dual-hit GE mice) had a similar somatic development (i.e. body weight and body length) and reflexes during the first 2 postnatal weeks. With the onset of the pre-juvenile period during the third postnatal week, the weight of dual-hit GE mice decreased when compared with controls (9.04 ± 0.31 g vs. 10.15 ± 0.31 g, $P = 0.02$), suggesting that with age the combination of risk genetic background and environmental stressors causes certain physical disability.

Pre-Juvenile Dual-Hit GE Mice Have Poorer Recognition Memory

Since adult mice with disease-related genetic background that experienced an early environmental stressor have poorer mnemonic and executive abilities (Abazyan et al. 2010; Ibi et al. 2010; Lipina et al. 2013), we first aimed at determining whether these cognitive deficits are present already during development. For this, we characterized the cognitive performance in controls, one-hit G, one-hit E, and dual-hit GE mice at pre-juvenile age [postnatal day (P) 16–24]. This developmental period shortly precedes the time window of adolescence that has been extensively investigated in human prodromal cohorts (Feinberg 1982; Keshavan et al. 2014; Selemon and Zecevic 2015). We specifically tested the four groups of mice in their behavioral abilities relying on the functional communication within hippocampal–prefrontal networks. Novelty detection and recognition memory, particularly temporal order memory (RR), have been identified to result from interactions within complex networks, centered on the PFC and HP (Barker and Warburton 2011; Warburton and Brown 2015), and to require their correct maturation (Kruger et al. 2012). These cognitive abilities are among the earliest that develop in life and can be easily tested at pre-juvenile age, since they rely on the mouse's intrinsic exploratory drive to investigate novel stimuli and consequently, lack overt stress components, such as food or water deprivation and forced swimming. We tested pre-juvenile control, one-hit G, one-hit E, and dual-hit GE mice for NOR, OLR, and RR, using a custom-designed arena and objects of different size, texture, and color (Fig. 1A,B). In line with our previous data (Kruger et al. 2012), we initiated the investigation after full maturation of sensory and motor abilities required for processing of novelty (P17). During the familiarization trial for NOR, all mice spent equal time investigating the two objects placed in the arena. During the testing trial, control animals ($n = 18$) spent significantly longer time interacting with the novel object (69.04 ± 6.74%, $P = 0.02$) than with the familiar one (30.96 ± 6.74%) and the mean duration of each interaction was also longer for the novel object (1.84 ± 0.32 s vs. 1.05 ± 0.12 s for familiar object, $P = 0.005$). In contrast, dual-hit GE mice ($n = 14$) did not distinguish between the two objects (familiar: 42.92 ± 9.15%; 1.83 ± 0.30 s; novel: 57.08 ± 9.15%, 1.87 ± 0.37 s, $P = 0.41$ and $P = 0.77$, respectively) (Fig. 1C, Supplementary Table 1). The behavioral impairment of one-hit mice did not follow a clear pattern. While one-hit E mice ($n = 9$) performed as well as controls, one-hit G mice ($n = 14$) were unable to recognize the novel object (Supplementary Fig. 1A). In contrast to the poorer performance of dual-hit GE and one-hit G mice in the NOR task, the OLR was intact in all four groups of mice (Fig. 1D, Supplementary Fig. 1B, Supplementary Table 1). While during the familiarization trial, they spent equal time investigating the two objects placed in the arena, during the test trial they spent significantly longer time interacting with the relocated object (control: 64.21 ± 5.39%, $n = 18$, $P = 0.02$, dual-hit GE: 62.94 ± 5.51%, $n = 15$, $P = 0.04$, one-hit E: 71.55 ± 6.41%, $n = 9$, $P = 0.01$, one-hit G: 69.19 ± 4.67%, $n = 15$, $P = 0.004$) than with the object with constant position (control: 35.78 ± 5.39%, dual-hit GE: 37.06 ± 5.51%, one-hit E: 28.45 ± 6.41%, one-hit G: 30.8 ± 4.67%). During the RR task, the pre-juvenile mice had to process temporal information by recognizing the object with which they most recently interacted (Fig. 1E, Supplementary Table 1). The control animals ($n = 16$) spent longer time with the object they explored during the first familiarization trial (recent: 36.9 ± 8.50%, old: 63.10 ± 8.50%, $P = 0.04$). Dual-hit GE mice ($n = 14$) failed to recognize the most recently explored object and equally investigated both objects (recent: 54.41 ± 7.4%, old: 45.59 ± 7.4%, $P = 0.41$). In contrast, one-hit E mice ($n = 14$) spent significantly more time with the object they explored during the first familiarization trial (recent: 39.02 ± 5.91%, old: 60.98 ± 5.91%, $P = 0.014$), whereas one-hit G mice ($n = 15$) equally explored the two objects (recent: 49.82 ± 5.27%, old: 50.18 ± 5.27%, $P = 0.96$).

The incapacity to achieve the NOR and RR tasks may result from poorer motor abilities and/or enhanced anxiety when interacting with the objects. To test this hypothesis, we first analyzed the exploratory behavior of P16 mice in the open field (Supplementary Table 2). The velocity and distance covered by

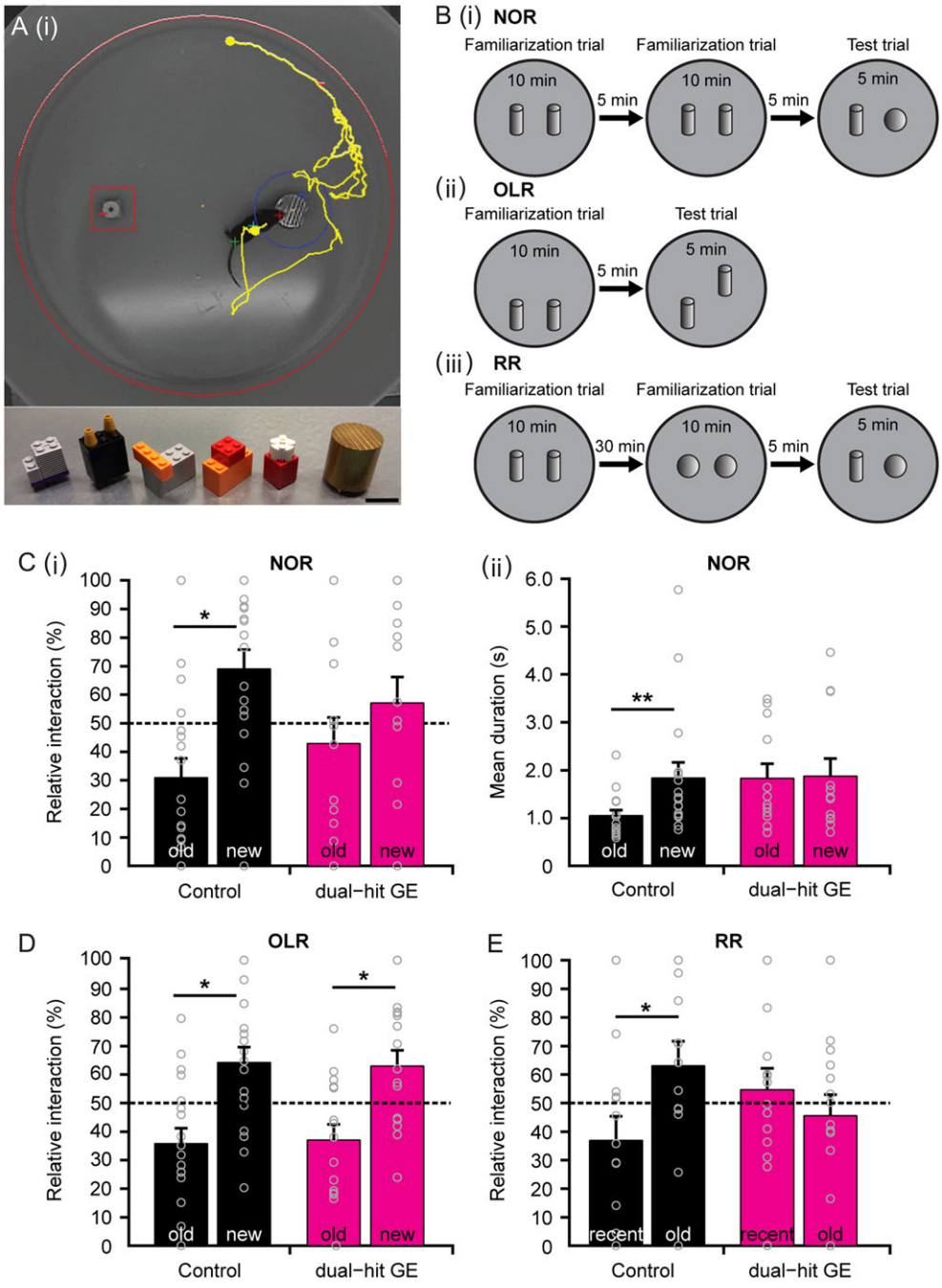

Figure 1. Impaired recognition memory of pre-juvenile dual-hit GE mice. (*A*) (i) Photograph of the arena used for testing novel object and OLR. The computer generated track of the mouse pup (yellow) is displayed together with zones (red, blue) created around the objects. (ii) Photograph of the objects with different textures, colors, shapes, and sizes that were used for NOR in pre-juvenile mouse pups. Scale bar: 2 cm. (*B*) Schematic diagrams of the protocol for (i) NOR, (ii) OLR, and (iii) RR tasks. (*C*) (i) Bar diagram illustrating the relative interaction time spent by control (n = 18, black) and dual-hit GE (n = 14, magenta) mice with the objects during the NOR test trial. The dotted line indicates chance level. (ii) Bar diagram illustrating the mean duration of a visit at the objects for control (black) and dual-hit GE (magenta) mice during the NOR test trial. (*D*) Same as (*C*) (i) for control (n = 18, black) and dual-hit GE (n = 15, magenta) mice in the OLR test trial. (*E*) Same as (*C*) (i) for control (n = 16, black) and dual-hit GE (n = 14, magenta) mice in the RR test trial. In (*C*–*E*) gray circles correspond to individual values. Data displayed as mean ± s.e.m.

controls (n = 17) and dual-hit GE mice (n = 14) were similar (3.54 ± 0.35 cm/s vs. 4.22 ± 0.36 cm/s, P = 0.22; 2121.81 ± 211.85 cm vs. 2530.44 ± 219.73 cm, P = 0.21). Animals from both groups spent equal time in the inner and outer circles of the arena and had similar latencies when entering the open field (76.34 ± 26.11 s vs. 28.81 ± 6.07 s, P = 0.44), suggesting that anxiety behavior of dual-hit GE mice was not enhanced. Furthermore, wall rearing, jumping, and grooming were comparable between the groups (Supplementary Table 2). Similarly, neither the horizontal nor the vertical locomotor activity of one-hit E or G mice was abnormal (Supplementary Table 2). Only one-hit E mice showed increased grooming frequency and decreased latency to groom versus controls. Moreover, the speed and total distance covered during the NOR

testing phase were similar in all four groups of mice (Supplementary Table 1). They did not show differences in the latency of the first contact with the objects either (Supplementary Table 1). Taken together, these results indicate that already at pre-juvenile age some cognitive abilities relying on hippocampal–prefrontal networks, such as item recognition and temporal order recognition, are impaired in dual-hit GE mice, whereas their exploratory and anxiety behavior is not affected. Similar early cognitive impairment is present in pre-juvenile one-hit G mice, but not in one-hit E mice. Of note, OLR that predominantly relies on hippocampal activation (Barker and Warburton 2011) is not affected in any of the models, suggesting that their HP has an intact function at pre-juvenile age.

The Oscillatory Coupling Within Hippocampal–Prefrontal Networks Is Augmented in Pre-Juvenile Dual-Hit GE Mice

The poorer performance in NOR task may indicate that at pre-juvenile age the function of hippocampal–prefrontal networks is impaired. To test this hypothesis, the behavioral investigation was succeeded by the examination of activity patterns in the PL and CA1 area of the intermediate HP, which have previously been reported to be densely coupled by axonal afferents and directed interactions during cognitive processing (Siapas et al. 2005; Hyman et al. 2010; Colgin 2011; Spellman et al. 2015). For this, we performed multi-site extracellular recordings of LFP and MUA simultaneously from PL and hippocampal CA1 area of urethane-anesthetized P22–24 controls ($n = 12$), dual-hit GE ($n = 11$), one-hit G ($n = 11$), and one-hit E ($n = 8$) mice (Fig. 2).

All investigated mice showed similar patterns of network activity, which correspond to the previously described sleep-like rhythms mimicked by urethane anesthesia (Wolansky et al. 2006; Clement et al. 2008; Pagliardini et al. 2013). Large-amplitude slow oscillations were superimposed with oscillatory activity in theta (4–12 Hz) and gamma (30–100 Hz) frequency range (Fig. 2Aii, iii, Bii, iii). These patterns were more prominent in the CA1 area of HP, where also sharp waves reversing over Str. pyramidale were regularly observed (Brockmann et al. 2011). We focused our analysis on the theta and gamma-band activity patterns, since they have been identified as a substrate of functional communication between PFC and HP during memory tasks (Benchenane et al. 2010; Hyman et al. 2010; Colgin 2011; Harris and Gordon 2015; Spellman et al. 2015). The amplitude and power of these patterns were similar in dual-hit GE mice when compared with controls (Supplementary Table 3). Prelimbic and hippocampal oscillatory activity in theta and gamma frequency range had comparable amplitude and power in control, dual-hit GE, and one-hit G mice. Only the prelimbic theta activity in one-hit E mice was mildly decreased when compared with controls and dual-hit GE animals.

Next, we tested whether the communication within hippocampal–prefrontal networks of one-hit and dual-hit mice was altered. First, we assessed the coupling by synchrony of both areas and calculated the coherence between LFP in PL and HP (Fig. 3A). Control mice showed a dominant peak in theta coherence between 4 and 12 Hz that was significantly larger than the peak for time-shuffled data (0.04 ± 0.01, 0.002 ± 0.00003, $P = 0.001$). Dual-hit GE mice also displayed significant hippocampal–prelimbic synchrony in the theta range; however, the coherence was significantly ($P = 0.037$) augmented (0.08 ± 0.01) when compared with values from control (0.04 ± 0.01) and one-hit E mice (0.03 ± 0.01, $P = 0.005$). In contrast, theta coherence in one-hit G and one-hit E mice was similar to the values from control animals (Supplementary Fig. 2A, Supplementary Table 4). Second, we confirmed this exaggerated communication within hippocampal–prefrontal networks in dual-hit GE mice by calculating the MI of theta–gamma phase-amplitude coupling of either amplitude in PL to hippocampal theta phase in HP or vice versa (Fig. 3B). All MIs were above chance level. In control animals, highest phase-amplitude coupling indicated by MI (original data: $5.80 \times 10^{-5} \pm 1.16 \times 10^{-5}$, significance threshold: $4.49 \times 10^{-6} \pm 2.18 \times 10^{-7}$) was observed for the coupling of prelimbic gamma amplitude to hippocampal theta phase. In dual-hit GE mice, the level of CFC was globally increased, most prominently for prelimbic gamma to hippocampal theta (original data: $9.79 \times 10^{-5} \pm 1.43 \times 10^{-5}$, significance threshold: $4.91 \times 10^{-6} \pm 5.31 \times 10^{-7}$, $P = 0.04$) as well as for theta amplitude in HP to theta phase in PL (controls, original data: $4.92 \times 10^{-6} \pm 7.75 \times 10^{-7}$, significance threshold: $2.74 \times 10^{-6} \pm 1.29 \times 10^{-7}$, dual-hit GE, original data: $1.15 \times 10^{-5} \pm 2.20 \times 10^{-6}$, significance threshold: $2.79 \times 10^{-6} \pm 2.31 \times 10^{-7}$, $P = 0.008$). In contrast, theta–gamma phase-amplitude coupling between PL and HP was similar in one-hit G, one-hit E, and control animals (Supplementary Fig. 2B). Only one-hit G mice showed increased coupling of theta amplitude in HP to theta phase in PL (controls, original data: $4.92 \times 10^{-6} \pm 7.75 \times 10^{-7}$, significance threshold: $2.74 \times 10^{-6} \pm 1.29 \times 10^{-7}$, one-hit G, original data: $9.14 \times 10^{-6} \pm 1.17 \times 10^{-6}$, significance threshold: $2.57 \times 10^{-6} \pm 1.43 \times 10^{-7}$, $P = 0.006$). These data indicate that despite similar patterns of oscillatory activity, the PL and HP are hyper-coupled by synchrony in dual-hit GE mice and to a certain amount also in one-hit G mice.

Due to its symmetric interdependence, the coherence does not offer reliable insights into the direction of information flow between the PL and the HP. To assess the directed interactions within hippocampal–prelimbic networks, we calculated the cross-correlation of instantaneous amplitudes of theta-band LFP in PL and HP and determined the time lag between them. This method allows to reliably infer directed interactions independent of spike sampling (Adhikari et al. 2010). Control mice showed a peak of maximal cross-correlation (0.198 ± 0.027) at a positive time lag of 16.15 ± 5.0 ms (Fig. 3C), confirming the monosynaptic drive from the CA1 area to PL (Brockmann et al., 2011) similar to adult animals (Adhikari et al. 2010). Dual-hit GE mice displayed maximal cross-correlation at a similar monosynaptic lag of 15.9 ± 2.0 ms but the peak was significantly increased when compared with control (0.32 ± 0.025, $P = 0.0051$) and one-hit E mice (0.17 ± 0.021, $P = 0.002$). Thus, in line with the hyper-synchrony, the directed hippocampal–prelimbic coupling is augmented in dual-hit GE mice. The directed interactions within hippocampal–prelimbic networks of one-hit G mice were slightly, but not significantly increased in their maximal cross-correlation and interaction delays when compared with controls, whereas in the one-hit E mice they remained unaltered (Supplementary Fig. 2C, Supplementary Table 4).

These results indicate that already at pre-juvenile age the coupling within hippocampal–prelimbic networks of dual-hit GE and, to a milder extent also of one-hit G mice, is abnormally augmented. To correlate the behavioral performance of each pre-juvenile mouse with the strength of hippocampal–prefrontal coupling, we calculated the discrimination ratio during the test phase (time spent at novel object minus time spent at familiar object divided by total interaction time) in relationship to the theta-band coherence. We found a significant anti-correlation for the RR test (Pearson's correlation −0.49, $P = 0.006$), but not for NOR (Pearson's correlation −0.072, $P = 0.7$) (Fig. 3D). These results strengthen the conclusion that

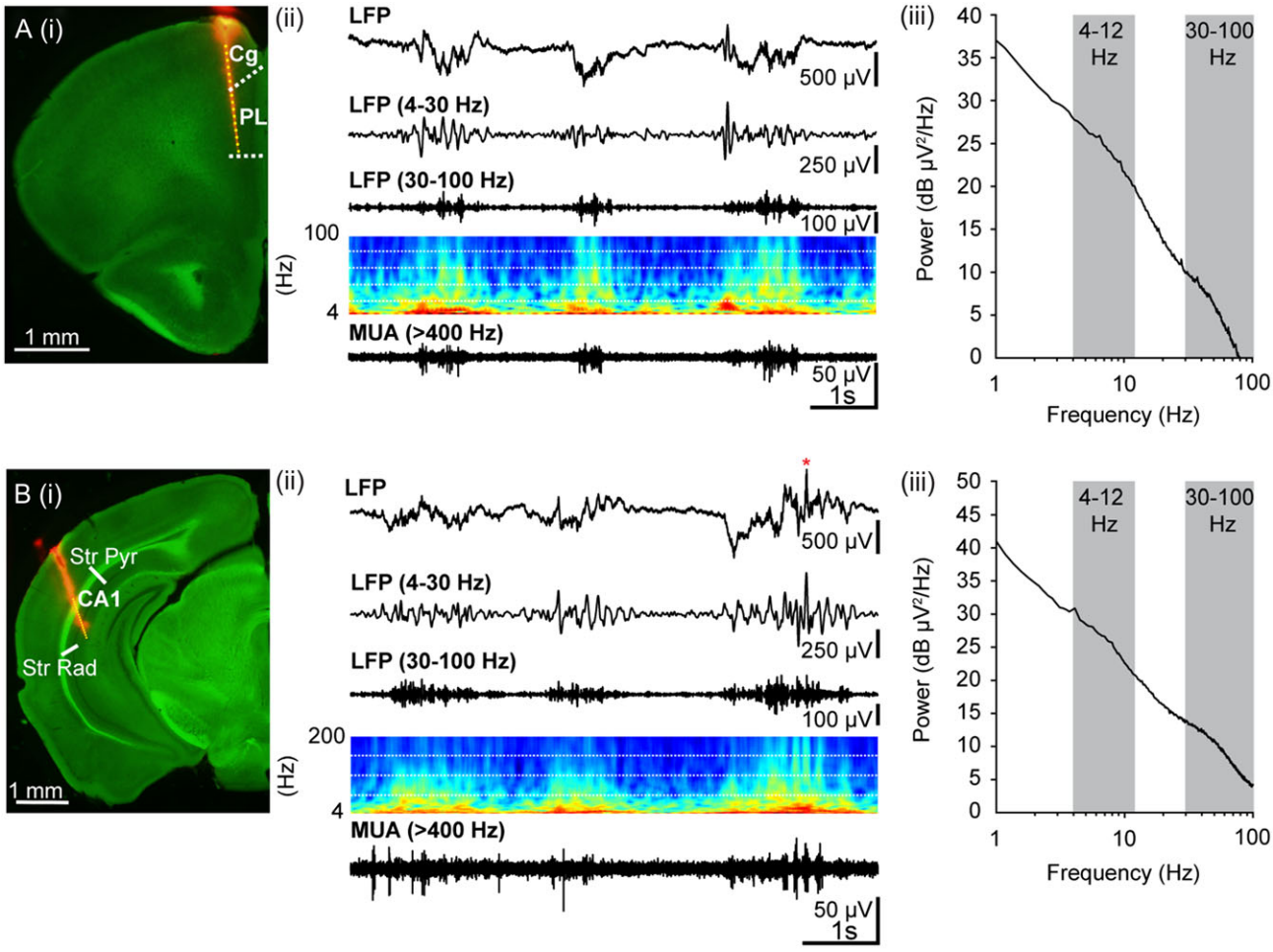

Figure 2. Oscillatory activity in PL and hippocampal CA1 area of pre-juvenile control mice. (*A*) (i) Digital photomontage reconstructing the location of the DiI-labeled recording electrode (orange) in PFC of a 75-µm-thick coronal section from a P23 mouse. The superimposed yellow dots mark the 16 recording sites covering the prefrontal subdivisions, cingulate cortex (Cg) and PL. (ii) Extracellular LFP recording of the oscillatory activity in PL from a P22 mouse displayed after band-pass (4–30 Hz, 30–100 Hz) filtering and accompanied by the corresponding MUA after 400 Hz high-pass filtering. At this age, the activity has switched to a continuous pattern of discharge with predominant slow oscillations and superimposed activity in the theta and gamma frequency range. Color-coded frequency plots show the wavelet spectra at identical time scale. (iii) Representative logarithmic power spectrum of an LFP recording in PL of a P23 mouse illustrating the broad power peaks in theta (4–12 Hz) and gamma (30–100 Hz, gray-shaded areas) frequency ranges. (*B*) (i) Digital photomontage reconstructing the location of the DiI-labeled recording electrode (orange) in the HP of a 75-µm-thick coronal section from a P23 mouse. The superimposed yellow dots mark the 16 recording sites covering stratum pyramidale (Str Pyr) and radiatum (Str Rad). (ii) Same as (*A*) (ii) for hippocampal LFP and MUA. Red asterisk marks sharp wave-ripple complex. (iii) Same as (*A*) (iii) for a representative hippocampal LFP recording.

abnormally augmented hippocampal–prefrontal coupling correlates with impaired temporal order memory.

The Patterns of Network Activity in the Neonatal PL and HP of Dual-Hit GE, But Not One-Hit Mice Are Disturbed Already at Neonatal Age

Since abnormal coupling by synchrony and augmented theta drive from the HP to PL in dual-hit GE mice is present at pre-juvenile age, it is likely that the network dysfunction resulting from the combination of genetic and environmental risk factors emerges prior to this late developmental period. To test this hypothesis, we investigated the four groups of mice at neonatal age (P8–10), the earliest developmental stage at which PL and HP functionally interact. We previously characterized the developmental profile of hippocampal–prelimbic interactions under normal conditions and showed that theta activity in CA1 area starts to unidirectionally entrain the local prelimbic circuits in beta-low gamma rhythms toward the end of the first postnatal week, reaching the maximal coupling at P8–10 (Brockmann et al. 2011).

We first characterized the activity patterns in PL and CA1 area of the intermediate HP, which in contrast to the rather continuous pre-juvenile discharge, are highly fragmented at neonatal age (Hanganu et al. 2006; Brockmann et al. 2011; Hartung et al. 2016). Extracellular recordings of LFP and MUA in lightly-anesthetized controls (PL: n = 16 animals, HP: n = 15 animals) followed by analysis using previously-developed unsupervised algorithm for detection and classification of oscillatory patterns (Cichon et al. 2014) confirmed the discontinuous aspect of neonatal activity (Fig. 4). In the PL, two major patterns were identified: SB with a single theta-band-confined frequency component (3–14 Hz), and NG with two distinct theta and beta-low gamma-confined frequency components (3–14 Hz, 14–30 Hz), which were superimposed with low-amplitude nested HFOs (100–400 Hz) (Fig. 4C, Supplementary Table 5).

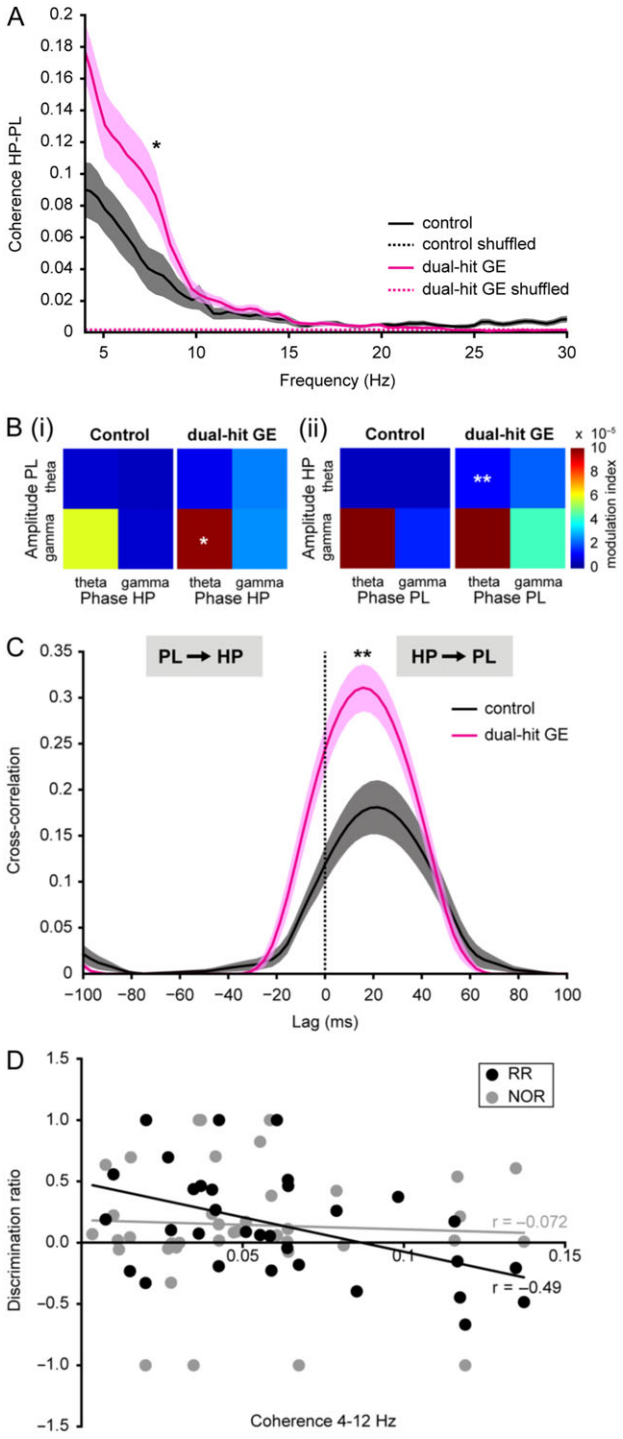

Figure 3. Hyper-coupling by synchrony and directed interactions within hippocampal–prelimbic networks of pre-juvenile dual-hit GE mice. (*A*) Averaged coherence spectra for simultaneously occurring oscillations in HP and PL of control (n = 12, black) and dual-hit GE mice (n = 11, magenta) for original (straight line) and time-shuffled (dotted line) data. (*B*) (i) Color-coded plots displaying the mean MI for the CFC of oscillation amplitudes in PL to the hippocampal phase in control (n = 12, left) and dual-hit GE (n = 11, right) mice. (ii) Same as (i) for CFC of amplitudes in the HP to the prelimbic phase. (*C*) Cross-correlations of the amplitudes of theta-filtered LFP recorded from PL and HP averaged for all investigated control (n = 12, black) and dual-hit GE mice (n = 11, magenta). Positive time lags correspond to HP leading the PL. (*D*) Diagram displaying the relationship between hippocampal–prefrontal coherence and behavioral performance in NOR (n = 40, gray) and RR task (n = 32, black) assessed as discrimination ratio between the two objects (i.e. difference between the time with novel object and the time with familiar object divided by total time of object exploration). The regression lines are plotted in the corresponding colors (black for RR, gray for NOR). In (*A*) and (*C*), the transparent areas correspond to s.e.m. *P < 0.05 and **P < 0.01.

These oscillatory patterns were accompanied by MUA, the prelimbic neurons showing the highest firing rate during NG (Supplementary Table 5). Similarly, the CA1 area of the intermediate HP was entrained in discontinuous network oscillations, which according to their dominant frequency within theta-band (3–14 Hz) were classified as theta bursts (Supplementary Table 6). Almost half of them (45.22 ± 5.76%) were accompanied by prominent sharp waves (Fig. 4*F*). These discontinuous patterns of oscillatory activity recorded under light urethane anesthesia mirror the network entrainment during sleep-like state (Clement et al. 2008), which represents the dominant physiological state of neonatal rodents. Correspondingly, they were similar to the activity patterns recorded from non-anesthetized asleep rodents (Bitzenhofer et al. 2015).

To decide whether genetic, environmental, and combined risk factors of neuropsychiatric disorders perturb the prelimbic and hippocampal activity already at neonatal age, we compared the network oscillations and neuronal firing in controls, dual-hit GE as well as one-hit G and one-hit E mice. While prelimbic SB and NG as well as hippocampal theta bursts are present in all investigated pups, their properties differed significantly between groups. The most prominent changes affected the dual-hit GE mice (PL: n = 12 animals, HP: n = 11 animals). The augmented occurrence of their SB (5.7 ± 0.5 events/min; controls 3.9 ± 0.5, P = 0.037) was accompanied by a strong decrease in amplitude (69.1 ± 3.8 μV; controls 92.1 ± 7.2 mV, P = 0.001) and power, especially within the NG-characteristic beta-low gamma frequency band (relative power: 6.7 ± 0.6; controls 14.9 ± 2.1, P = 0.0001) (Fig. 5*A*,*B*, Supplementary Table 5). Moreover, the firing of prelimbic neurons was significantly (P < 0.001) increased in dual-hit GE mice (0.39 ± 0.04 Hz; controls 0.17 ± 0.02 Hz, P < 0.0001) and less neurons were phase-locked to a distinct phase of gamma activity. However, the locking strength of firing did not significantly change in the PL of dual-hit GE mice (Supplementary Fig. 3*A*–*C*). Similar perturbation of network activity, that is, significantly higher occurrence (6.5 ± 0.4 events/min; controls 3.8 ± 0.4 events/min, P < 0.0001) and lower oscillatory power in theta frequency (relative power 15.2 ± 2.3; controls: 25.2 ± 3.5, P = 0.029), was found when the hippocampal theta bursts were analyzed in dual-hit GE mice (Fig. 5*C*,*D*, Supplementary Table 6). Moreover, the firing rate of hippocampal neurons was increased, but despite a constant number of phase-locked neurons, their timing by the theta rhythm was weaker (Supplementary Fig. 3*D*–*F*, Supplementary Table 6). These alterations in network oscillations and spiking patterns in PL and hippocampal CA1 of dual-hit GE mice were significant when related not only to controls, but also to one-hit mice (Supplementary Figs 4 and 5, Supplementary Tables 5 and 6). In contrast to the prominent changes in dual-hit GE mice, the prelimbic and hippocampal activity of one-hit G (n = 9) and one-hit E (PL: n = 22, HP: n = 18) mice was largely normal, although the occurrence of hippocampal theta bursts in one-hit E mice, their firing rates during both SB and NG in PL, as well as firing rate of hippocampal neurons in one-hit G mice were slightly increased when compared with controls (Supplementary Fig. 6, Supplementary Table 6).

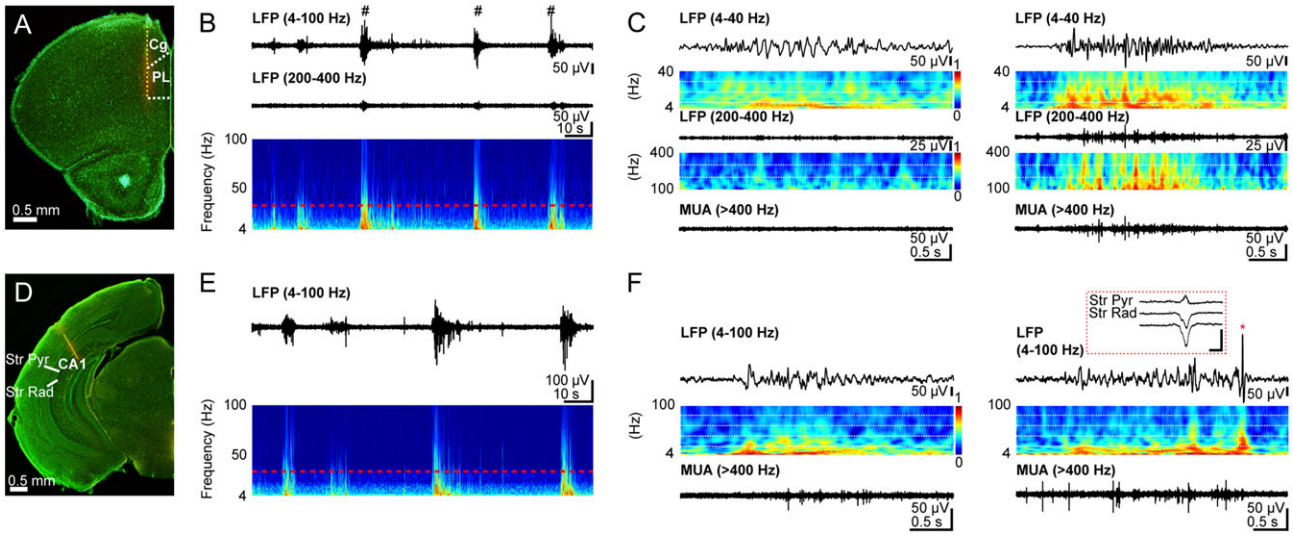

Figure 4. Patterns of oscillatory activity in PL and hippocampal CA1 area of neonatal control mice. (*A*) Digital photomontage reconstructing the location of the DiI-labeled recording electrode (orange) in PFC of a Nissl-stained 75-μm-thick coronal section from a P10 mouse. The superimposed yellow dots mark the 16 recording sites covering the prefrontal subdivisions, cingulate cortex (Cg) and PL. (*B*) Extracellular LFP recording of discontinuous oscillatory activity in PL from a P10 mouse displayed after band-pass (4–100 Hz, 200–400 Hz) filtering. Traces are accompanied by the color-coded wavelet spectra of the LFP at identical time scale. The red-dotted line indicates the lower border of the gamma frequency range (30 Hz). NG characterized by a wide frequency distribution and superimposed HFOs (200–400 Hz) are marked by hashes. (*C*) Left: Characteristic SB displayed after band-pass (4–40 Hz and 200–400 Hz) filtering and the corresponding MUA after 400 Hz high-pass filtering. Color-coded frequency plots show the wavelet spectra at identical time scale. Right: Characteristic NG displayed after band-pass (4–40 Hz and 200–400 Hz) filtering and the corresponding MUA after 400 Hz high-pass filtering. Color-coded frequency plots show the wavelet spectra at identical time scale. Note the presence of prominent beta-low gamma episodes with nested HFOs that are accompanied by strong spike discharge. (*D*) Same as (*A*) for recording electrode in hippocampal CA1. The superimposed yellow dots mark the 16 recording sites covering stratum pyramidale (Str Pyr) and radiatum (Str Rad). (*E*) Same as (*B*) for hippocampal LFP. (*F*) Left: Characteristic theta burst displayed after band-pass (4–100 Hz) filtering accompanied by the corresponding MUA after 400 Hz high-pass filtering and the color-coded frequency plot at identical time scale. Right: Characteristic theta burst with sharp wave (red asterisk) displayed after band-pass (4–100 Hz) filtering accompanied by the corresponding MUA after 400 Hz high-pass filtering and the color-coded frequency plot at identical time scale. Inset, sharp wave reversing between Str Pyr and Str Rad and displayed at a larger time scale. Scale bars for inset correspond to 200 μV and 0.1 s.

These findings demonstrate that the combination of genetic and environmental risk factors of major neuropsychiatric disorders profoundly disturbs and disorganizes the network activity of the neonatal PL and hippocampal CA1, whereas the oscillatory patterns are largely unaffected when the two risk factors do not converge.

The Synchrony Within Neonatal Hippocampal-Prelimbic Networks Is Impaired in Dual-Hit GE, But Not in One-Hit Mice

To test whether genetic and environmental risk factors affect the coupling between neonatal PL and HP, we first examined the hippocampal–prelimbic synchrony for simultaneously recorded network oscillations and spikes in the PL and CA1 area of all four groups of mice. While at adulthood, coupling of brain areas by synchrony is necessary for behavioral performance (Jones and Wilson 2005), during development it seems to represent the pre-requisite for correct network wiring (Brockmann et al. 2011; Minlebaev et al. 2011). The fraction of co-occurring prelimbic and hippocampal events was significantly decreased in dual-hit GE mice (83 ± 1.6%, $n = 15$, $P = 0.039$) and one-hit E mice (76.4 ± 3.6%, $n = 17$, $P = 0.034$), but similar in one-hit G mice (87.3 ± 1.9%, $n = 6$, $P = 0.91$) when compared with controls (86.6 ± 1.3%, $n = 16$). Calculation of the coherence in different frequency bands (3–8 Hz, 8–14 Hz, and 14–30 Hz) showed tight synchrony within hippocampal–prelimbic networks of control pups already at this immature age (Supplementary Table 7). This was a genuine feature of hippocampal–prelimbic interactions and not the result of non-specific/volume-conducted synchrony, since the values of the imaginary part of coherence within 8–14 Hz and 14–30 Hz were similar (S Bitzenhofer, C Lindemann, IL Hanganu-Opatz, unpublished data) and time shuffling significantly decreased the coherence of prelimbic and hippocampal oscillations (Fig. 6*A*) as well as the coherence between prelimbic LFP and individual hippocampal spikes (Fig. 6*B*) (Soteropoulos and Baker 2006).

In dual-hit GE mice, the hippocampal–prelimbic coherence was significantly lower (8–14 Hz: 0.04 ± 0.01; 14–30 Hz: 0.06 ± 0.01) when compared with controls (8–14 Hz: 0.09 ± 0.02, $P = 0.013$; 14–30 Hz: 0.1 ± 0.02, $P = 0.04$) (Fig. 6*C*,*D*, Supplementary Table 7), one-hit E mice (8–14 Hz: 0.09 ± 0.01, $P < 0.0001$; 14–30 Hz: 0.11 ± 0.02, $P = 0.014$) (Supplementary Fig. 5*E*,*F*), and one-hit G mice (8–14 Hz: 0.11 ± 0.03, $P = 0.005$) (Supplementary Fig. 4*E*,*F*). The changes principally affected the frequency range of hippocampal theta bursts (3–14 Hz), which have been previously identified as functional drive for the oscillatory entrainment of local prelimbic networks (Brockmann et al. 2011). The synchrony deficits of dual-hit GE mice were confirmed by the decrease in coherence between prelimbic oscillations and hippocampal spikes (Fig. 6*E*). In contrast, the coupling by synchrony of hippocampal–prelimbic networks in mice mimicking either the genetic or environmental risk factors was not perturbed. The coherence over the entire frequency spectrum was similar in one-hit G, one-hit E, and control mice (Supplementary Fig. 7*A*,*B*, Supplementary Table 7).

These data indicate that the combination of genetic and environmental risk factors diminishes theta synchrony between the neonatal PL and hippocampal CA1, whereas the

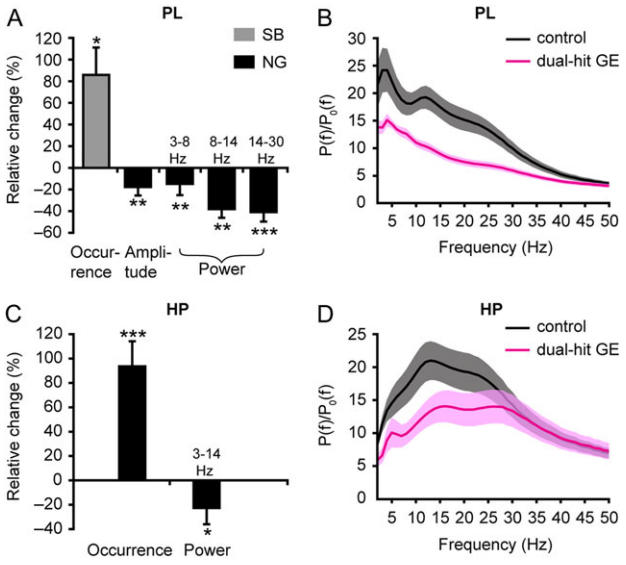

Figure 5. Abnormal patterns of discontinuous oscillatory activity in PL and HP of neonatal dual-hit GE mice. (*A*) Bar diagrams displaying the relative changes in the occurrence, amplitude, and power in different frequency bands of prelimbic SB (gray) and NG (black) from dual-hit GE mice ($n = 12$) when related to values of controls ($n = 16$). (*B*) Averaged power spectra $P(f)$ of discontinuous oscillations (NG) normalized by the baseline power $P_0(f)$ of time windows lacking activity when displayed for controls (black) and dual-hit GE mice (magenta). (*C*) Same as (*A*) for theta bursts recorded in the CA1 area of the intermediate HP (controls: $n = 15$, dual-hit GE mice: $n = 11$). (*D*) Same as (*B*) for hippocampal theta bursts. In (*A*) and (*C*), only significant differences were displayed and positive values indicate an increase, whereas negative values indicate a decrease when compared with controls. $^*P < 0.05$, $^{**}P < 0.01$, $^{***}P < 0.001$. Data shown as mean ± s.e.m.

oscillatory coupling between the two areas is not modified when the risk factors do not converge.

The Directed Interactions Within Neonatal Hippocampal–Prelimbic Networks Are Weaker in Dual-Hit GE, But Not in One-Hit Mice

To assess the directed interactions within neonatal hippocampal–prelimbic networks, we used two different approaches. In a first step, we calculated the cross-correlation of instantaneous amplitudes of filtered LFP in the PL and HP of P8–10 mice. For control mice ($n = 21$), the maximal cross-correlation (0.164 ± 0.013) was obtained at a positive time lag of 15.6 ± 2.2 ms (Fig. 7A), confirming the monosynaptic drive from the CA1 area to PL, which has been previously identified in neonatal rats (Brockmann et al. 2011). This first cross-correlation peak was followed by a second one at longer positive lag of ~46 ms, suggesting that polysynaptic interactions complemented the monosynaptic influence of the HP on PL. Additionally, feedback coupling seems to indirectly relay information from PL back to HP, because a small, but significant peak of cross-correlation (0.015 ± 0.006) was detected in controls at a negative time lag of –62.5 ± 2.5 ms. In dual-hit GE mice ($n = 12$), the prominent monosynaptic drive from HP to PL strongly decreased, as shown by the significant ($P = 0.004$) reduction of the cross-correlation peak at 15.6 ± 3.4 ms to 0.089 ± 0.019 ms. In contrast, the peaks corresponding to polysynaptic and feedback interactions were similar or even augmented (e.g. peak at ~78 ms) when compared with controls. Moreover, the positive values of cross-correlation corresponding to directed interactions from HP to PL had a broader distribution. The diminishment and loss of precision of directed interactions within neonatal hippocampal–prelimbic networks were exclusively present when the genetic and environmental risk factors converged as confirmed also by the significantly decreased cross-correlation in dual-hit GE mice when compared with one-hit E mice ($n = 18$) (Supplementary Fig. 5G). Neither the monosynaptic drive from the HP to PL nor the polysynaptic feedback interactions were modified in the neonatal one-hit G ($n = 6$) and one-hit E mice (Supplementary Fig. 8A,B, Supplementary Table 7).

In a second step, we confirmed the disruption of directed interactions within neonatal hippocampal–prelimbic networks in dual-hit GE mice by assessing the temporal relationship between hippocampal and prelimbic firing. For this, we calculated the cross-correlation of spike trains recorded in PL and HP (Brillinger 1976; Halliday and Rosenberg 1999; Siapas et al. 2005) (Fig. 7B). If the HP directly drives the PL, then the prelimbic neurons will fire shortly (i.e. at the lag of monosynaptic projections) after the hippocampal ones. Despite the fact that the low firing rates and number of recorded neurons, which are characteristic for the immature PL and HP at neonatal age, hampered the analysis, a small but reliable peak of cross-correlation between the spike trains has been detected at a positive lag of ~20 ms ($n = 325$ cell pairs from 13 mice, Fig. 7C). This indicates that in control mice, the HP indeed directly drives the PL. The same peak was present also in dual-hit GE mice ($n = 72$ cell pairs from 11 mice); however, its magnitude was decreased. These data confirm the causality analysis of LFP oscillations and suggest that the timing of prelimbic firing by the hippocampal discharge via monosynaptic projections is disturbed in dual-hit GE mice.

Thus, a combination of genetic and environmental risk factors of neuropsychiatric disorders causes a major decrease in neonatal theta drive from the CA1 area to the PL. In contrast, the early directed interactions remain intact when the risk factors do not converge.

Discussion

Disrupted synchrony and abnormal oscillatory entrainment within adult hippocampal–prefrontal networks have been proposed as underlying mechanism of cognitive impairment in neurodevelopmental psychiatric disorders, such as schizophrenia (Meyer-Lindenberg et al. 2005; Sigurdsson et al. 2010; Godsil et al. 2013). In the present study, we combined multi-site recordings from neonatal and pre-juvenile mice modeling the disorder etiology with their behavioral investigation to elucidate at which developmental time point and by which mechanisms the maturation of hippocampal–prefrontal networks is impaired. We demonstrate here that 1) at neonatal and pre-juvenile age the functional interactions within hippocampal–prefrontal networks are disturbed when genetic and environmental risk factors of disease converge and to a lesser extent when they act separately; 2) already at neonatal age the network activity is temporally uncoordinated and the initial interactions between PL and HP are weaker in dual-hit GE mice; 3) the neonatal hypo-coupling in these mice switches during pre-juvenile development to an augmented communication within hippocampal–prelimbic networks; similar, but milder effects can also be observed in one-hit G mice; 4) dual-hit GE and one-hit G mice have already at pre-juvenile age poorer cognitive abilities that correlate with the degree of abnormal interactions between PL and HP (Fig. 8). These data identify the de-coupling of hippocampal–prefrontal networks during early development followed by their exaggerated communication at pre-juvenile

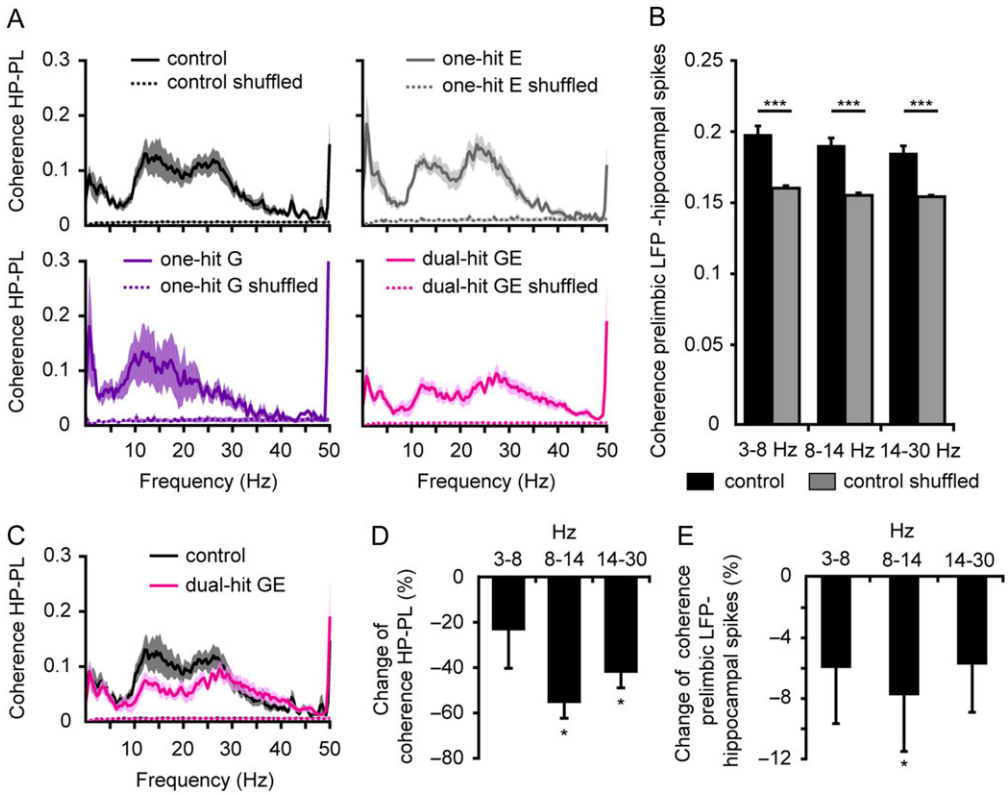

Figure 6. Reduced coupling by synchrony within hippocampal–prelimbic networks of neonatal dual-hit GE mice. (*A*) Mean coherence spectra for original (solid line) and time-shuffled (dotted line) network oscillations simultaneously recorded in neonatal PL and HP of controls ($n = 16$, black), one-hit G ($n = 6$, violet), one-hit E ($n = 17$, gray), and dual-hit GE mice ($n = 15$, magenta). (*B*) Bar diagram displaying the mean coherence in different frequency bands for LFP oscillations in PL and original and time-shuffled spikes in HP of controls ($n = 14$). (*C*) Coherence spectra for co-occurring network oscillations in neonatal PL and HP when averaged for all controls (black) and dual-hit GE mice (magenta). (*D*) Bar diagram displaying the relative changes in the coherence for co-occurring prelimbic and hippocampal oscillations in dual-hit GE mice when related to coherence values of controls. (*E*) Same as (*D*) for coherence of prelimbic LFP and hippocampal spikes. In (*D*) and (*E*), positive values indicate an increase, whereas negative values indicate a decrease when compared with controls. *$P < 0.05$ and ***$P < 0.001$. Data shown as mean ± s.e.m.

age as a potential mechanism of adult disease-related circuit dysfunction and cognitive impairment.

Animal Models of Major Neuropsychiatric Disorders

Understanding mental illness has been mainly hampered by the difficulties of generating animal models that capture all features of an extremely heterogeneous group of disorders, including schizophrenia and major depression. However, when scaling such ambitious goals down and focusing on one or few features, mouse models represent valuable tools, especially for elucidating the circuit dysfunction as neurobiological substrate of these diseases (Arguello and Gogos 2006; Nestler and Hyman 2010; Wong and Josselyn 2015). The most widely used models mimic the human etiology of disease, the susceptibility of genetic modifications, and the action of environmental stressors. While disease-relevant phenotypes have been identified for these factors acting alone, their combination has been proposed as reflecting more accurately the human pathology (van Os and Kapur 2009; Insel 2010; van Os et al. 2010).

In the present study, we used mouse models that have been extensively characterized at adulthood. They have been confirmed to mimic certain cognitive deficits and/or the dysfunction of hippocampal–prefrontal networks reported for mental disorders, yet their deficits are rather mild. On the one hand, the one-hit G mouse model carries one of the few well-defined DISC1 risk alleles, which has been linked in a large human pedigree not only to schizophrenia (Millar et al. 2000; Koike et al. 2006), but also more broadly to mental illness (Farrell et al. 2015). *DISC1* is critically involved in neurogenesis, migration of pyramidal neurons and interneurons as well as circuit formation (Kamiya et al. 2005; Mao et al. 2009; Lipina and Roder 2014). Its mutation affects in a highly selective fashion synaptic plasticity and causes social, sensory-motor, and cognitive deficits at adulthood (Kvajo et al. 2008). Our data showed that already at pre-juvenile age one-hit G mice had poorer recognition and temporal order memory and mild alterations of network interactions. However, the dysfunction seems to emerge quite late during development, since at neonatal age one-hit G mice were almost indistinguishable from controls in their activity patterns, coupling by synchrony or directed communication within hippocampal–prefrontal networks.

On the other hand, we used prenatal immune challenge induced by poly (I:C) treatment as environmental stressor. Adult one-hit E mice showed decreased hippocampal–prefrontal synchrony and abnormal related cognitive behavior (Dickerson et al. 2010). In line with previous reports (Meyer and Feldon 2012), we observed that functional and behavioral deficits are not present at early stages of development, neither the patterns of activity and coupling within hippocampal–prefrontal networks nor the behavior being altered in one-hit E mice during neonatal and pre-juvenile development.

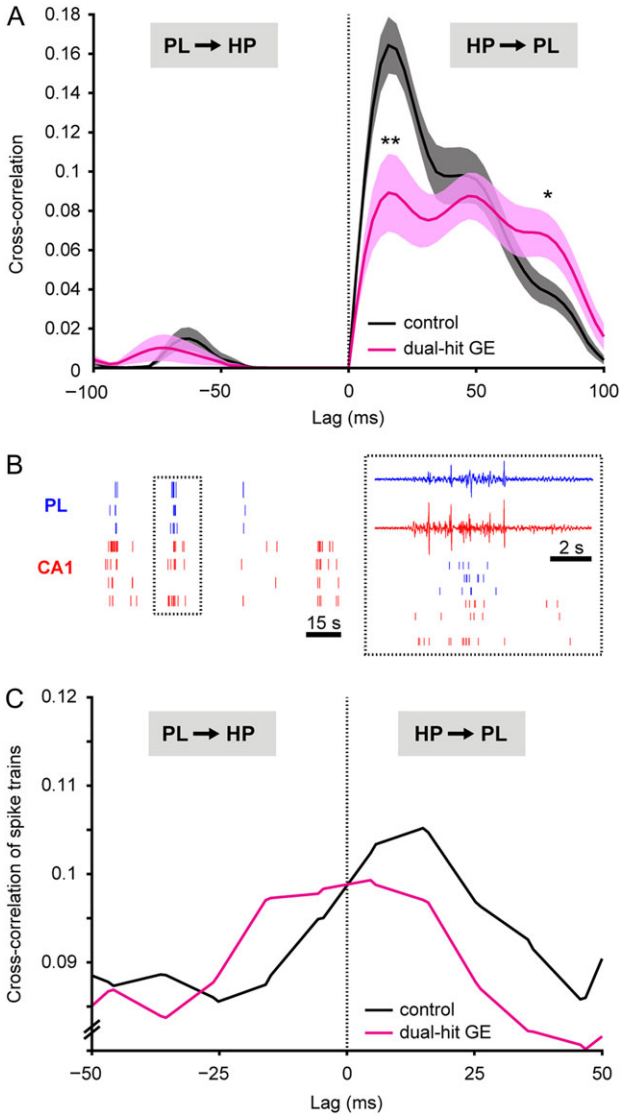

Figure 7. Abnormal directed interactions between PL and HP of neonatal dual-hit GE mice. (*A*) Amplitude cross-correlation of prelimbic and hippocampal network oscillations averaged for all investigated controls (n = 21, black) and dual-hit GE mice (n = 12, magenta). Positive time lags correspond to HP leading PL. *$P < 0.05$, **$P < 0.01$. Data shown as mean ± s.e.m. (*B*) Examples of spike trains from 3 prelimbic (blue) and 4 hippocampal (red) neurons simultaneously recorded from a P8 control. Inset, close-up of the spike trains displayed together with the corresponding LFP reveals the confinement of spikes to time windows of network oscillations. (*C*) Cross-correlation histograms of hippocampal–prelimbic spike trains recorded from controls (n = 325 cell pairs from 13 mice, black) and dual-hit GE mice (n = 72 cell pairs from 11 mice, magenta). Positive time lags correspond to HP leading PL.

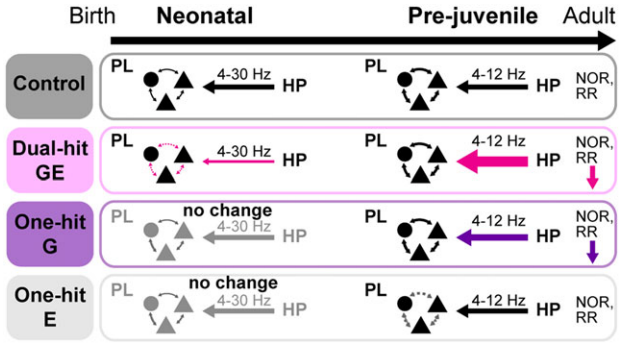

Figure 8. Schematic diagram of age-dependent hippocampal–prelimbic interactions in control, dual-hit GE, one-hit G, and one-hit E mice.

Given the fact that, differently from the adult phenotype, neither the genetic nor the environmental risk factors alone impaired the network communication at neonatal age, it is surprising that their combination leads to a profound diminishment of coupling by synchrony and reduction of theta hippocampal drive to PL. One possibility is that *Disc1* mutation may induce perturbation of immune-relevant signaling pathways early in life (Beurel et al. 2010). The resulting structural, cellular, and behavioral deficits might persist and even augment throughout the life span, altered cognitive and social behavior, anxiety, and hyperactivity being detected at adult age (Abazyan et al. 2010; Ibi et al. 2010; Lipina et al. 2013).

Periods of High Vulnerability in Major Neuropsychiatric Disorders

Identification of developmental periods of vulnerability to functional and behavioral dysfunctions in neuropsychiatric disorders represents one major aim, but also challenge of research (van Os et al. 2010). Clinical studies proposed two time windows of structural and functional organization of neuronal maturation as critical for mental illness. First, the middle-late stage of pregnancy in humans, which corresponds to neonatal age in rodents (Clancy et al. 2001), has been associated with an increased risk of major neuropsychiatric disorders (Cannon and Murray 1998; Lewis and Levitt 2002; Jones et al. 2014), because the developing neuronal networks undergoing substantial refinement at this age are particularly prone to several environmental risk factors. However, the early development has been largely factored out from experimental investigations of the cellular and circuit substrate of neuropsychiatric disorders, mainly due to major ethical concerns and technical limitations. Our previous studies revealed that the emergence of first long-range coupling within the brain takes place during neonatal development (Brockmann et al. 2011). At the end of the first postnatal week, the functional entrainment of neonatal PL in discontinuous oscillatory rhythms is initiated by the hippocampal theta-timed activity. The directed communication within neonatal hippocampal–prefrontal networks is necessary for the later ontogeny of cognitive processing (Kruger et al. 2012). Consequently, its dysfunction as a result of co-acting genetic and environmental risk factors might lead to abnormal/delayed wiring of PL and HP that persists until adulthood and underlie the poorer mnemonic and executive performance.

The disease-relevant dysfunction of neuronal networks during the neonatal development might be potentiated during the second time window with critical relevance for mental illness. Disturbances in brain maturation during adolescence have been proposed to contribute to the pathophysiology of schizophrenia (Feinberg 1982; Weinberger 1987; Keshavan et al. 1994). During this late developmental stage, profound re-organization of neural circuits as a result of connectivity pruning and excitation/inhibition changes takes place during physiological conditions. The power and phase synchrony over a wide range of frequencies decrease (Srinivasan 1999; Whitford et al. 2007). In the mouse models analyzed here, combination of genetic and environmental risk factors and to a lesser extent also the abnormal genetic background alone appear to perturb this

process of maturation. Shortly before the onset of adolescence, the theta-band coupling between PL and HP is augmented in dual-hit GE mice. The exaggerated entrainment might result from aberrant pruning of connectivity. The present data confirm the critical role of pre-juvenile/adolescent age for mental illness and give first insights into the mechanisms by which the peri- and prenatal risk factors impact the developing long-range circuitry.

Mechanisms and Physiological Relevance of Abnormal Hippocampal-Prelimbic Communication During Development for Mental Illness

The present results reveal that the network dysfunction in neuropsychiatric disorders, while occurring during the entire development, has distinct age-dependent patterns. At neonatal age reduced theta synchrony and directed interactions caused de-coupling of prefrontal and hippocampal activity in dual-hit GE, but not in one-hit mice (Fig. 8). Assessment of functional communication at comparable age in humans (for example, second-third gestational trimester) is ethically and technically not feasible, yet future investigations of other mouse models might reveal whether the de-coupling between PFC and HP is a "finger print" of disease. Most likely, these alterations in network activity in theta-band reflected a global perturbation of brain activity due to the combined action of genetic and environmental factors on cortical migration and differentiation. Structural changes, such as a decrease in spine density or lower number of axonal terminals, might lead to augmentation of the firing of pyramidal neurons in the hippocampal CA1 area, but also to loss of theta-timed precision of firing, as reflected by the weaker strength of theta-spike coupling. The disorganized activation of HP and the weaker drive to PL might be accompanied by a reduction in axonal projections between the two areas. These structural and functional deficits may perturb the prelimbic activity and initial wiring of local circuits. Activation of neonatal prelimbic interneurons by glutamatergic inputs, most likely from pyramidal CA1 neurons, has been identified as a cellular substrate for the entrainment of local circuits in gamma-band oscillatory rhythms (Bitzenhofer et al. 2015). Consequently, disease-specific alterations in glutamatergic-GABAergic interplay may decrease the power of local gamma oscillations in the PL and the timing precision of prelimbic firing by gamma activity.

In contrast, at pre-juvenile age, an augmented theta-band synchrony and driving force was identified to exaggeratedly entrain the PL and HP of dual-hit GE mice (Fig. 8). The increase in hippocampal–prefrontal coupling goes far beyond a normal compensation of directionality strength between the two areas. Moreover, it is not related to a memory task as reported in adults (Jones and Wilson 2005; Sigurdsson et al. 2010), since it has been detected in anesthetized pre-juvenile mice. However, the general degree of hyper-coupling though correlates well with the behavioral impairment of individual animals in temporal order memory, suggesting that even impaired coupling at baseline affects cognitive task performance. Around the onset of clinical symptoms, both at resting state and during cognitive tasks hippocampal–prefrontal hypoconnectivity and decreased beta-gamma synchrony have been identified as the major disease-related markers in patients (Meyer-Lindenberg et al. 2005; Uhlhaas and Singer 2011; Benetti et al. 2015; Cui et al. 2015). Correspondingly, the cognitive abilities relying on hippocampal–prefrontal coupling such as object-in-place recognition are impaired in dual-hit GE mice of comparable age (adolescent–young adult) (C Lindemann, IL Hanganu-Opatz, unpublished observations). These functional deficits have been proposed to result from myelination defects, modification of GABAergic neurotransmission and alteration in the expression of specific genes (Salami et al. 2003; Harris et al. 2009; Hashimoto et al. 2009). Since the fast-spiking parvalbumin-positive interneurons are the driving force of gamma-band activity (Cardin et al. 2009; Sohal et al. 2009), their hypofunction may account for the observed diminishment of gamma synchrony in prodromal cohorts and first-episode patients. Further investigations are warranted to monitor in detail the transition from pre-juvenile hyper-coupling to the adolescent/adult hypo-coupling. Another key question that needs to be addressed concerns the exact identity of cellular elements and interactions that account for disease-relevant dysfunction of hippocampal–prefrontal networks during neonatal and pre-juvenile development. Manipulation of specific neuronal populations in the immature circuits will provide first insights into the cellular mechanisms of disease's ontogeny.

Identification of a developmental switch from hypo- to hyper-coupling within neuronal networks as a new pathophysiological mechanism of neuropsychiatric disorders may open new therapeutic perspectives that, when initiated before the onset of clinical symptoms, may improve the devastating cognitive outcome of disease (Dawson et al. 2015).

Author Contributions

I.L.H.-O. designed the experiments, C.M. contributed to experimental design, J.A.G. engineered and provided the mice, H.H., S.R., S.S., and C.L. carried out the experiments, H.H., N.C., and V.D.F analyzed the data, I.L.H.-O., H.H., and V.D.F interpreted the data and wrote the paper. All authors discussed and commented on the manuscript.

Supplementary Material

Supplementary material can be found at: http://www.cercor.oxfordjournals.org/.

Funding

German Research Foundation (SFB 936 B5 to I.L.H.-O. and C6 to C.M., Emmy Noether-Program to I.L.H.-O. and Priority Program 1665 to I.L.H.-O.) and the European Research Council (FP7-ERC CoG 681577 PSYCHOCELL to I.L.H.-O.).

Notes

We thank A. Marquardt and A. Dahlmann for excellent technical assistance, Dr I. Hermans-Borgmeyer for help with mice breeding and maintenance, Drs A. Wolff and M. Muhia for help with the design of one-hit E model. *Conflict of Interest*: Drs Hartung, Cichon, De Feo, Lindemann, Mulert, Gogos and Hanganu-Opatz as well as S. Riemann and S. Schildt have no biomedical financial interests or potential conflicts of interest to declare related to the present study.

References

Abazyan B, Nomura J, Kannan G, Ishizuka K, Tamashiro KL, Nucifora F, Pogorelov V, Ladenheim B, Yang C, Krasnova IN, et al. 2010. Prenatal interaction of mutant DISC1 and immune activation produces adult psychopathology. Biol Psychiatry. 68:1172–1181.

Adhikari A, Sigurdsson T, Topiwala MA, Gordon JA. 2010. Cross-correlation of instantaneous amplitudes of field potential oscillations: a straightforward method to estimate the directionality and lag between brain areas. J Neurosci Methods. 191:191–200.

Arguello PA, Gogos JA. 2006. Modeling madness in mice: one piece at a time. Neuron. 52:179–196.

Barker GR, Warburton EC. 2011. When is the hippocampus involved in recognition memory? J Neurosci. 31: 10721–10731.

Benchenane K, Peyrache A, Khamassi M, Tierney PL, Gioanni Y, Battaglia FP, Wiener SI. 2010. Coherent theta oscillations and reorganization of spike timing in the hippocampal- prefrontal network upon learning. Neuron. 66:921–936.

Benetti S, Pettersson-Yeo W, Allen P, Catani M, Williams S, Barsaglini A, Kambeitz-Ilankovic LM, McGuire P, Mechelli A. 2015. Auditory verbal hallucinations and brain dysconnectivity in the perisylvian language network: a multimodal investigation. Schizophr Bull. 41:192–200.

Beurel E, Michalek SM, Jope RS. 2010. Innate and adaptive immune responses regulated by glycogen synthase kinase-3 (GSK3). Trends Immunol. 31:24–31.

Bitzenhofer SH, Sieben K, Siebert KD, Spehr M, Hanganu-Opatz IL. 2015. Oscillatory activity in developing prefrontal networks results from theta-gamma-modulated synaptic inputs. Cell Rep. 11:486–497.

Blackwood DH, Fordyce A, Walker MT, St Clair DM, Porteous DJ, Muir WJ. 2001. Schizophrenia and affective disorders–cosegregation with a translocation at chromosome 1q42 that directly disrupts brain-expressed genes: clinical and P300 findings in a family. Am J Hum Genet. 69:428–433.

Brandon NJ, Sawa A. 2011. Linking neurodevelopmental and synaptic theories of mental illness through DISC1. Nat Rev Neurosci. 12:707–722.

Brillinger DM. 1976. Estimation of the second-order intensities in a bivariate stationary point process. J R Stat Soc. 38: 60–66.

Brockmann MD, Poschel B, Cichon N, Hanganu-Opatz IL. 2011. Coupled oscillations mediate directed interactions between prefrontal cortex and hippocampus of the neonatal rat. Neuron. 71:332–347.

Cannon M, Murray RM. 1998. Neonatal origins of schizophrenia. Arch Dis Child. 78:1–3.

Cannon TD, van Erp TG, Bearden CE, Loewy R, Thompson P, Toga AW, Huttunen MO, Keshavan MS, Seidman LJ, Tsuang MT. 2003. Early and late neurodevelopmental influences in the prodrome to schizophrenia: contributions of genes, environment, and their interactions. Schizophr Bull. 29:653–669.

Cardin JA, Carlen M, Meletis K, Knoblich U, Zhang F, Deisseroth K, Tsai LH, Moore CI. 2009. Driving fast-spiking cells induces gamma rhythm and controls sensory responses. Nature. 459: 663–667.

Cash-Padgett T, Jaaro-Peled H. 2013. DISC1 mouse models as a tool to decipher gene-environment interactions in psychiatric disorders. Front Behav Neurosci. 7:113.

Cichon NB, Denker M, Grun S, Hanganu-Opatz IL. 2014. Unsupervised classification of neocortical activity patterns in neonatal and pre-juvenile rodents. Front Neural Circuits. 8:50.

Clancy B, Darlington RB, Finlay BL. 2001. Translating developmental time across mammalian species. Neuroscience. 105: 7–17.

Clement EA, Richard A, Thwaites M, Ailon J, Peters S, Dickson CT. 2008. Cyclic and sleep-like spontaneous alternations of brain state under urethane anaesthesia. PLoS One. 3:e2004.

Colgin LL. 2011. Oscillations and hippocampal-prefrontal synchrony. Curr Opin Neurobiol. 21:467–474.

Cui LB, Liu J, Wang LX, Li C, Xi YB, Guo F, Wang HN, Zhang LC, Liu WM, He H, et al. 2015. Anterior cingulate cortex-related connectivity in first-episode schizophrenia: a spectral dynamic causal modeling study with functional magnetic resonance imaging. Front Hum Neurosci. 9:589.

Dawson N, Morris BJ, Pratt JA. 2015. Functional brain connectivity phenotypes for schizophrenia drug discovery. J Psychopharmacol. 29:169–177.

Dickerson DD, Wolff AR, Bilkey DK. 2010. Abnormal long-range neural synchrony in a maternal immune activation animal model of schizophrenia. J Neurosci. 30:12424–12431.

Ennaceur A, Delacour J. 1988. A new one-trial test for neurobiological studies of memory in rats. 1: Behavioral data. Behav Brain Res. 31:47–59.

Farrell MS, Werge T, Sklar P, Owen MJ, Ophoff RA, O'Donovan MC, Corvin A, Cichon S, Sullivan PF. 2015. Evaluating historical candidate genes for schizophrenia. Mol Psychiatry. 20: 555–562.

Feinberg I. 1982. Schizophrenia: caused by a fault in programmed synaptic elimination during adolescence? J Psychiatr Res. 17:319–334.

Genzel L, Dresler M, Cornu M, Jager E, Konrad B, Adamczyk M, Friess E, Steiger A, Czisch M, Goya-Maldonado R. 2015. Medial prefrontal-hippocampal connectivity and motor memory consolidation in depression and schizophrenia. Biol Psychiatry. 77:177–186.

Godsil BP, Kiss JP, Spedding M, Jay TM. 2013. The hippocampal-prefrontal pathway: the weak link in psychiatric disorders? Eur Neuropsychopharmacol. 23:1165–1181.

Halliday DM, Rosenberg JR. 1999.Time and frequency domain analysis of spike train and time series data. In: Windhorst U, Johansson H, editors. Modern Techniques in Neuroscience Research. Berlin, Heidelberg, Germany: Springer. p. 503–543.

Hanganu IL, Ben-Ari Y, Khazipov R. 2006. Retinal waves trigger spindle bursts in the neonatal rat visual cortex. J Neurosci. 26:6728–6736.

Harris AZ, Gordon JA. 2015. Long-range neural synchrony in behavior. Annu Rev Neurosci. 38:171–194.

Harris LW, Lockstone HE, Khaitovich P, Weickert CS, Webster MJ, Bahn S. 2009. Gene expression in the prefrontal cortex during adolescence: implications for the onset of schizophrenia. BMC Med Genomics. 2:28.

Hartung H, Brockmann MD, Poschel B, De Feo V, Hanganu-Opatz IL. 2016. Thalamic and entorhinal network activity differently modulates the functional development of prefrontal-hippocampal interactions. J Neurosci. 36: 3676–3690.

Hashimoto T, Nguyen QL, Rotaru D, Keenan T, Arion D, Beneyto M, Gonzalez-Burgos G, Lewis DA. 2009. Protracted developmental trajectories of GABAA receptor alpha1 and alpha2 subunit expression in primate prefrontal cortex. Biol Psychiatry. 65: 1015–1023.

Heyser CJ, Ferris JS. 2013. Object exploration in the developing rat: methodological considerations. Dev Psychobiol. 55: 373–381.

Hu H, Gan J, Jonas P. 2014. Interneurons. Fast-spiking, parvalbumin(+) GABAergic interneurons: from cellular design to microcircuit function. Science. 345:1255263.

Hyman JM, Zilli EA, Paley AM, Hasselmo ME. 2010. Working memory performance correlates with prefrontal-hippocampal theta interactions but not with prefrontal neuron firing rates. Front Integr Neurosci. 4:2.

Ibi D, Nagai T, Koike H, Kitahara Y, Mizoguchi H, Niwa M, Jaaro-Peled H, Nitta A, Yoneda Y, Nabeshima T, et al. 2010. Combined effect of neonatal immune activation and mutant DISC1 on phenotypic changes in adulthood. Behav Brain Res. 206:32–37.

Insel TR. 2010. Rethinking schizophrenia. Nature. 468:187–193.

Jones I, Chandra PS, Dazzan P, Howard LM. 2014. Bipolar disorder, affective psychosis, and schizophrenia in pregnancy and the post-partum period. Lancet. 384:1789–1799.

Jones MW, Wilson MA. 2005. Theta rhythms coordinate hippocampal-prefrontal interactions in a spatial memory task. PLoS Biol. 3:e402.

Kamiya A, Kubo K, Tomoda T, Takaki M, Youn R, Ozeki Y, Sawamura N, Park U, Kudo C, Okawa M, et al. 2005. A schizophrenia-associated mutation of DISC1 perturbs cerebral cortex development. Nat Cell Biol. 7:1167–1178.

Keshavan MS, Anderson S, Pettegrew JW. 1994. Is schizophrenia due to excessive synaptic pruning in the prefrontal cortex? The Feinberg hypothesis revisited. J Psychiatr Res. 28: 239–265.

Keshavan MS, Giedd J, Lau JY, Lewis DA, Paus T. 2014. Changes in the adolescent brain and the pathophysiology of psychotic disorders. Lancet Psychiatry. 1:549–558.

Koike H, Arguello PA, Kvajo M, Karayiorgou M, Gogos JA. 2006. Disc1 is mutated in the 129S6/SvEv strain and modulates working memory in mice. Proc Natl Acad Sci USA. 103: 3693–3697.

Kruger HS, Brockmann MD, Salamon J, Ittrich H, Hanganu-Opatz IL. 2012. Neonatal hippocampal lesion alters the functional maturation of the prefrontal cortex and the early cognitive development in pre-juvenile rats. Neurobiol Learn Mem. 97:470–481.

Kvajo M, McKellar H, Arguello PA, Drew LJ, Moore H, MacDermott AB, Karayiorgou M, Gogos JA. 2008. A mutation in mouse Disc1 that models a schizophrenia risk allele leads to specific alterations in neuronal architecture and cognition. Proc Natl Acad Sci USA. 105:7076–7081.

Kvajo M, McKellar H, Drew LJ, Lepagnol-Bestel AM, Xiao L, Levy RJ, Blazeski R, Arguello PA, Lacefield CO, Mason CA, et al. 2011. Altered axonal targeting and short-term plasticity in the hippocampus of Disc1 mutant mice. Proc Natl Acad Sci USA. 108:E1349–1358.

Lee FH, Zai CC, Cordes SP, Roder JC, Wong AH. 2013. Abnormal interneuron development in disrupted-in-schizophrenia-1 L100P mutant mice. Mol Brain. 6:20.

Lewis DA, Levitt P. 2002. Schizophrenia as a disorder of neurodevelopment. Annu Rev Neurosci. 25:409–432.

Lipina TV, Roder JC. 2014. Disrupted-In-Schizophrenia-1 (DISC1) interactome and mental disorders: impact of mouse models. Neurosci Biobehav Rev. 45:271–294.

Lipina TV, Zai C, Hlousek D, Roder JC, Wong AH. 2013. Maternal immune activation during gestation interacts with Disc1 point mutation to exacerbate schizophrenia-related behaviors in mice. J Neurosci. 33:7654–7666.

Mao Y, Ge X, Frank CL, Madison JM, Koehler AN, Doud MK, Tassa C, Berry EM, Soda T, Singh KK, et al. 2009. Disrupted in schizophrenia 1 regulates neuronal progenitor proliferation via modulation of GSK3beta/beta-catenin signaling. Cell. 136:1017–1031.

Meyer-Lindenberg AS, Olsen RK, Kohn PD, Brown T, Egan MF, Weinberger DR, Berman KF. 2005. Regionally specific disturbance of dorsolateral prefrontal-hippocampal functional connectivity in schizophrenia. Arch Gen Psychiatry. 62:379–386.

Meyer U, Feldon J. 2012. To poly(I:C) or not to poly(I:C): advancing preclinical schizophrenia research through the use of prenatal immune activation models. Neuropharmacology. 62:1308–1321.

Meyer U, Feldon J, Schedlowski M, Yee BK. 2005. Towards an immuno-precipitated neurodevelopmental animal model of schizophrenia. Neurosci Biobehav Rev. 29:913–947.

Millar JK, Wilson-Annan JC, Anderson S, Christie S, Taylor MS, Semple CA, Devon RS, St Clair DM, Muir WJ, Blackwood DH, et al. 2000. Disruption of two novel genes by a translocation co-segregating with schizophrenia. Hum Mol Genet. 9: 1415–1423.

Minlebaev M, Colonnese M, Tsintsadze T, Sirota A, Khazipov R. 2011. Early gamma oscillations synchronize developing thalamus and cortex. Science. 334:226–229.

Nestler EJ, Hyman SE. 2010. Animal models of neuropsychiatric disorders. Nat Neurosci. 13:1161–1169.

Pagliardini S, Gosgnach S, Dickson CT. 2013. Spontaneous sleep-like brain state alternations and breathing characteristics in urethane anesthetized mice. PloS One. 8:e70411.

Pletnikov MV, Ayhan Y, Nikolskaia O, Xu Y, Ovanesov MV, Huang H, Mori S, Moran TH, Ross CA. 2008. Inducible expression of mutant human DISC1 in mice is associated with brain and behavioral abnormalities reminiscent of schizophrenia. Mol Psychiatry. 13:173–186115.

Reichenberg A, Caspi A, Harrington H, Houts R, Keefe RS, Murray RM, Poulton R, Moffitt TE. 2010. Static and dynamic cognitive deficits in childhood preceding adult schizophrenia: a 30-year study. Am J Psychiatry. 167:160–169.

Salami M, Itami C, Tsumoto T, Kimura F. 2003. Change of conduction velocity by regional myelination yields constant latency irrespective of distance between thalamus and cortex. Proc Natl Acad Sci USA. 100:6174–6179.

Sauer JF, Struber M, Bartos M. 2015. Impaired fast-spiking interneuron function in a genetic mouse model of depression. Elife. 4.

Schmidt MJ, Mirnics K. 2015. Neurodevelopment, GABA system dysfunction, and schizophrenia. Neuropsychopharmacology. 40:190–206.

Selemon LD, Zecevic N. 2015. Schizophrenia: a tale of two critical periods for prefrontal cortical development. Transl Psychiatry. 5:e623.

Shi L, Fatemi SH, Sidwell RW, Patterson PH. 2003. Maternal influenza infection causes marked behavioral and pharmacological changes in the offspring. J Neurosci. 23:297–302.

Siapas AG, Lubenov EV, Wilson MA. 2005. Prefrontal phase locking to hippocampal theta oscillations. Neuron. 46:141–151.

Sigurdsson T, Stark KL, Karayiorgou M, Gogos JA, Gordon JA. 2010. Impaired hippocampal-prefrontal synchrony in a genetic mouse model of schizophrenia. Nature. 464:763–767.

Sohal VS, Zhang F, Yizhar O, Deisseroth K. 2009. Parvalbumin neurons and gamma rhythms enhance cortical circuit performance. Nature. 459:698–702.

Song W, Li W, Feng J, Heston LL, Scaringe WA, Sommer SS. 2008. Identification of high risk DISC1 structural variants with a 2% attributable risk for schizophrenia. Biochem Biophys Res Commun. 367:700–706.

Song W, Li W, Noltner K, Yan J, Green E, Grozeva D, Jones IR, Craddock N, Longmate J, Feng J, et al. 2010. Identification of

high risk DISC1 protein structural variants in patients with bipolar spectrum disorder. Neurosci Lett. 486:136–140.
Soteropoulos DS, Baker SN. 2006. Cortico-cerebellar coherence during a precision grip task in the monkey. J Neurophysiol. 95:1194–1206.
Spellman T, Rigotti M, Ahmari SE, Fusi S, Gogos JA, Gordon JA. 2015. Hippocampal-prefrontal input supports spatial encoding in working memory. Nature. 522:309–314.
Srinivasan R. 1999. Spatial structure of the human alpha rhythm: global correlation in adults and local correlation in children. Clin Neurophysiol. 110:1351–1362.
Taylor SF, Tso IF. 2014. GABA abnormalities in schizophrenia: a methodological review of in vivo studies. Schizophr Res. 167:84–90.
Tort AB, Komorowski R, Eichenbaum H, Kopell N. 2010. Measuring phase-amplitude coupling between neuronal oscillations of different frequencies. J Neurophysiol. 104: 1195–1210.
Uhlhaas PJ, Singer W. 2010. Abnormal neural oscillations and synchrony in schizophrenia. Nat Rev Neurosci. 11:100–113.
Uhlhaas PJ, Singer W. 2011. The development of neural synchrony and large-scale cortical networks during adolescence: relevance for the pathophysiology of schizophrenia and neurodevelopmental hypothesis. Schizophr Bull. 37:514–523.
van Os J, Kapur S. 2009. Schizophrenia. Lancet. 374:635–645.
van Os J, Kenis G, Rutten BP. 2010. The environment and schizophrenia. Nature. 468:203–212.
Warburton EC, Brown MW. 2015. Neural circuitry for rat recognition memory. Behav Brain Res. 285:131–139.
Weinberger DR. 1987. Implications of normal brain development for the pathogenesis of schizophrenia. Arch Gen Psychiatry. 44:660–669.
Wernicke C. 1906. Grundriss der Psychiatrie in klinischen Vorlesungen. Leipzig, Germany: Thieme.
White T, Ho BC, Ward J, O'Leary D, Andreasen NC. 2006. Neuropsychological performance in first-episode adolescents with schizophrenia: a comparison with first-episode adults and adolescent control subjects. Biol Psychiatry. 60: 463–471.
Whitford TJ, Rennie CJ, Grieve SM, Clark CR, Gordon E, Williams LM. 2007. Brain maturation in adolescence: concurrent changes in neuroanatomy and neurophysiology. Hum Brain Mapp. 28:228–237.
Wolansky T, Clement EA, Peters SR, Palczak MA, Dickson CT. 2006. Hippocampal slow oscillation: a novel EEG state and its coordination with ongoing neocortical activity. J Neurosci. 26:6213–6229.
Wong AH, Josselyn SA. 2015. Caution when diagnosing your mouse with schizophrenia: the use and misuse of model animals for understanding psychiatric disorders. Biol Psychiatry. 79:32–38.
Woodberry KA, Giuliano AJ, Seidman LJ. 2008. Premorbid IQ in schizophrenia: a meta-analytic review. Am J Psychiatry. 165: 579–587.